(1)

BERKELEY RESEARCH ASSOCIATES, INC.

BRA-88-334R
August 1988

COLLECTIVE FREE ELECTRON LASER THEORY

W. B. Colson
Berkeley Research Associates, Inc.
P. O. Box 241
Berkeley, CA 94701

Final Report
Contract No. N00014-86-C-2006

Prepared for
Naval Research Laboratory
Washington, DC 20375

BRA-88-334R
August 1988

COLLECTIVE FREE ELECTRON LASER THEORY

W. B. Colson

Berkeley Research Associates, Inc.

P. O. Box 241

Berkeley, CA 94701

Final Report

Contract No. N00014-86-C-2006

Prepared for

Naval Research Laboratory

Washington, DC 20375

STATEMENT "A" per Philip Sprangle
NRL/Code 4790
TELECON 4/20/90 VG

Final Report

Naval Research Laboratory Contract No. N00014-86-C-2006

October 30, 1985 to July 30, 1986

W. B. Colson

Introduction

The long-pulse induction linac at NRL [1-6] is considered for the first stage of a two-stage free electron laser (FEL) oscillator. This research effort studies several effects that can significantly influence the performance of such an FEL. The NRL FEL is parameterized in a set of dimensionless variables that can summarize several physical effects without the use of detailed calculation as well as relating the physical to other FEL designs. A waveguide analysis shows the primary modifications on the FEL interaction, electron beam distribution functions representing energy spread and emittance are evaluated in the high gain regime, and a multimode analysis of the trapped-particle instability is performed for parameters describing the NRL FEL. The research in intended to extend the simulation theory of high-gain FEL oscillators.

In the two-stage FEL, the first-stage uses a normal FEL interaction with the usual static undulator to produce an intense electromagnetic wave in a high-power resonator. The wavelength in the first stage is around 1cm, and provides the periodic undulator in the second stage of the interaction. The electromagnetic undulator has a shorter wavelength with a more intense field than can be attained from a static magnetic field, and allows the second stage to reach short optical wavelengths with a low energy electron beam. But, the performance of the two-stage FEL is completely determined by the all important first-stage. For this reason, the emphasis of this research is

concentrated on understanding the high power operation of the high-gain FEL oscillator.

Data and design parameters from the first six references below provide a physical description of the NRL FEL. Many physical variables like current and beam energy changed from experiment to experiment but remained in the general range described here. The NRL FEL uses a $\gamma mc^2 = 7\text{keV}$ electron beam so that $\gamma \approx 2.4$. The beam current I is about 200A in a beam radius of $r_e \approx 0.5\text{cm}$. Reference [4] gives the angular spread of the electron beam as $\Delta\theta \approx 0.014$, and there is a 2% energy spread. The undulator has a $\lambda_0 = 4\text{cm}$ period over $N = 22$ periods, and the peak field strength is $B = 625\text{Gauss}$ with helical polarization. The "undulator constant" for such an undulator is $K = eB\lambda_0/2\pi mc^2 \approx 0.23$. An $a = 3\text{cm}$ diameter waveguide confines the radiation to a small volume around the co-propagating electron beam. The lowest order mode has a beam radius of $w_0 \approx 0.8\text{cm}$. The combined waveguide, resonator, and output coupling loss each pass n is about 30%, so that in the absence of gain the optical field would decay as $\propto e^{-n/2Q}$ where $Q = 3 \rightarrow 4$. The long-pulse NRL accelerator provides current for about 2μs, or about $n = 200$ passes.

The filling factor $F = \pi r_e^2/\pi w_0^2 \approx 0.4$ describes the reduced coupling due to the mismatch in the electron beam and radiation beam sizes. The Rayleigh length for the radiation that would be emitted from the electron beam with no waveguide is much shorter than the interaction length $L = N\lambda_0 = 88\text{cm}$. It is shown below that this could significantly reduce coupling in the NRL FEL. The general criteria for the use of a waveguide in an FEL is derived.

The electron beam density $\rho = 5\times10^{10}\text{cm}^{-3}$ and the filling factor determine the dimensionless beam current $j = 8N(e\pi KL)^2\rho F/\gamma^3 mc^2 \approx 320$. When $j \gg 1$, the FEL has the potential for high exponential gain if there is sufficient beam quality. The weak field power gain is given by $G = e^{(j/2)^{1/3}\sqrt{3}}/9$ and is $G \approx 10^3$, or $G \approx 30\text{dB}$. These levels of amplification are in rough agreement with the experiment, but there is some degradation due to beam quality. The gain spectrum bandwidth is given by $\Delta_G \approx 4j^{1/6} \approx 2\pi$ for this

FEL.

For a low-energy, high-current electron beam, interparticle Coulomb forces can cause plasma oscillations to modify the simple FEL interaction mechanism. The relativistic plasma frequency is $\Omega_p = (4\pi e^2 \rho/\gamma^3 m)^{1/2} \approx 3\times10^9 s^{-1}$. The number of plasma oscillations during a passage of the beam through the undulator in the interaction time L/c is $N_{plasma} = \Omega_p L/2\pi c \approx 1.6$. This is larger than for most FEL experiments, but still small enough that the main interaction would be determined by the exponential growth described above.

Another unique feature of the NRL experiment is that it did not use a uniform guide field to contain the low-energy electron beam along the undulator. The helical undulator field focuses in both transverse dimensions and causes $N_\beta = NK/\gamma \approx 2.2$ betatron oscillations along the interaction length. Both the radius of the electron beam and the angular spread contribute to the spread in electron phase velocities during the interaction. Energy spread also deters bunching. To compare these effects on the same footing, they are all related to the gain spectrum bandwidth $1/2N$. For an angular spread of $\Delta\theta$ in a beam of radius r_e, the spread in electron phase velocities is given by

$$\sigma_\beta = 4\pi N\,(K^2 k_0^2 r_e^2 + \gamma^2\theta^2)/(1+K^2) \quad .$$

When $\sigma_\beta \approx \pi$, the spread in phase velocities is comparable to the gain spectrum bandwidth, and gain degradation becomes important. Both the angular spread and beam size contributions should be matched consistent with the beam emittance in order to optimize performance. In the NRL FEL, $\sigma_\beta \approx 8$ indicating there will be some loss of gain due to beam quality. More importantly, it is reported in several of the references that the position of the electron centered can be off of the undulator axis by as much as the beam radius 0.5cm. This causes a shift and a spread in the phase velocity distribution of the beam. The shift alone is $\Delta\sigma_\beta \approx 35$ and should cause dramatic changes in the interaction strength. In the high-gain regime, the shape of the electron

distribution function becomes extremely important in determining the interaction characteristics along the undulator. A much more detailed analysis of these features is covered in an appendix.

FELs using Waveguides

When an FEL uses a waveguide to confine the radiation along the undulator, there are changes to the simple FEL interaction. Usually the goal of the design is to make the changes as small as possible while confining the wave around the co-propagating electron beam.

General Criteria for the FEL Waveguide: When the FEL optical wavelength is long, free space diffraction can spread the optical wavefront away from the co-propagating electron beam and reduce coupling. The natural distance for a light beam of wavelength λ to double its initial beam area, πw_0^2, is the Rayleigh length $Z_0 = \pi w_0^2/\lambda$. Comparing this length to the undulator length L defines the dimensionless Rayleigh length $z_0 = \pi w_0^2/L\lambda$. Without a waveguide, the optical wavelength is determined by the resonance condition, $\lambda = \lambda_0(1+K^2)/2\gamma^2$ where $K = e\bar{B}\lambda_0/2\pi mc^2$ is the undulator parameter, $\lambda_0 = k_0/2\pi$ is the undulator wavelength, and γmc^2 is the electron beam energy. The Rayleigh length becomes $z_0 = 2\pi w_0^2\gamma^2/(1+K^2)N\lambda_0^2$, and expresses how an FEL with a low energy electron beam gives a short Rayleigh length.

A design attempting to compensate for low γ by expanding the optical beam size w_0 would suffer reduced coupling because of a small filling factor $F_0 = \pi r_e^2/w_0^2$; r_e is the electron beam radius. When natural diffraction spreads the optical wave away the electron beam the filling factor is reduced further; assuming the light remains in the lowest order Gaussian mode with its waist at the center of the undulator, the average filling factor over the undulator length is $\bar{F} = F_0/(1+1/12z_0^2)$, or $\bar{F} = \sigma_e^2/(z_0+1/12z_0)$ where $\sigma_e = r_e(\pi/L\lambda)^{1/2}$ is the dimensionless electron beam radius. Typically, $\sigma_e \approx 1$ in an FEL, but the following arguments are independent of that value and only depend on the

Rayleigh length z_0. For $z_0 \to 0$, $\bar{F} \to 0$ and coupling $\to 0$, because the optical wave spreads away from the electron beam at the two ends of the undulator; for $z_0 \to \infty$, $\bar{F} \to 0$ and coupling $\to 0$ again, because the wavefront is too large compared to electron beam. The maximum filling factor, $\bar{F}^{max} = F_0/2$, or $\bar{F}^{max} = \sqrt{3}\sigma_e^2$, occurs at $z_0^{max} = (12)^{-1/2}$. The maximum is relatively broad in z_0 and $\bar{F}^{max}$ drops to half of its peak value, $\sqrt{3}\sigma_e^2/2$, at $z_0 \approx 0.11$ and 0.75.

The filling factor could be increased for an optical wavefront of any size, if the electron beam size is increased. But, as the electrons move off of the undulator axis, approaching the undulator magnets, the field strength $\bar{B}$ increases and deflects electrons back towards the axis causing betatron oscillations. The extra transverse motion decreases z velocity of the relativistic electrons and changes the resonance condition. The change in the electron phase velocity in a matched beam with radius r_e is $\Delta v_\beta = 4\pi N (K k_0 r_e)^2/(1+K^2)$. Gain degradation begins when the beam radius is large enough to cause $\Delta v_\beta \approx \pi$. The limit on the beam radius for good coupling is then $r_e \lesssim (1+K^2)^{1/2}\lambda_0/4\pi K N^{1/2}$. Generally, a typical FEL has $N \approx 10^2$ so that the electron radius is restricted to a much smaller value than the undulator wavelength. For $K \approx 1$, we have $r_e \lesssim 0.01\lambda_0$, or for $K \ll 1$, we have $r_e \lesssim 0.01\lambda_0/K$.

The combination of (1) the restriction on the spread of electron phase velocities, or beam radius, and (2) the requirement of good coupling, or large filling factor F with a given optical beam size w_0, gives a restriction on the Rayleigh length in terms of γ and N. To relate r_e and w_0, assume that the filling factor is not too small, say $F > F_0 \geq 0.1$, so that $w_0 \lesssim 3r_e$. Then, the dimensionless Rayleigh length is limited by $z_0 \lesssim \gamma^2/\pi K^2 N^2$. Either a low energy beam or a long undulator can limit z_0 to a small value and decrease the filling factor. The limit is relaxed when K is small, because the electron beam can be expanded to support a wide optical wavefront without much diffraction. Gain degradation begins to occur when the coupling is reduced by small values of $\bar{F}$. The peak value of $\bar{F}$, $\sqrt{3}\sigma_e^2$, decreases to less than half its value when the limit above

restricts $z_0 \leq 0.1$. Therefore, an FEL design requires

$$\gamma \leq KN/2$$

so that natural diffraction does not significantly decrease the interaction strength. An FEL with low electron beam energy and a long, strong undulator, requires a waveguide for good coupling strength.

FEL Resonance in a Waveguide: When a waveguide is used to confine the radiation near the co-propagating electron beam there is a change in the FEL resonance condition. In a single waveguide mode, the cross-section of the mode can be used in the filling factor to estimate coupling to the mode. The electron beam size should be close to, but smaller than, the radiation cross-section for best coupling. Assuming the electron beam is on-axis, the mode should have a transverse electric field on-axis as well. Higher order modes will average to smaller coupling if the electron beam size is not much smaller than the mode. At NRL, the waveguide is cylindrical in cross-section with a $a = 1.5$cm radius. Since the electron beam size is about $r_e \approx 0.5$cm, and is comparable to the fundamental mode size, no more than 2 to 3 nodes should not couple well.

The time dependence of the waveguide fields is taken to be $\propto e^{-i\omega t}$ with longitudinal dependence $\propto e^{\pm ikz}$. Waveguide modes are separated into two classes: TE - transverse electric modes where the longitudinal component of the electric field $E_z = 0$ everywhere, and TM - transverse magnetic modes where the longitudinal component of the magnetic field $B_z = 0$ everywhere. At the waveguide wall, the TE mode boundary condition is $B_z' = 0$ while the TM mode boundary condition is $E_z = 0$. The waveguide cross-section and boundary conditions specify and eigenvalue problem with a number of eigenvalues Λ_p, where $p = 1,2,3,.....$ For a given frequency, the wave equation in the waveguide determines the wavenumber k_p for each value of p,

$$k_p^2 = \omega^2/c^2 - \Lambda_p^2 \quad .$$

When the frequency is below cut-off, $\omega/c \le \Lambda_p$, the wavenumber k_p is zero, or imaginary, and mode does not propagate; $\omega_p = c\,\Lambda_p$ is called the cut-off frequency of the waveguide.

All waveguide modes have the form $E_\perp \propto e^{\pm i k_p z - i\omega t}$. The backward propagating wave, $E_\perp \propto e^{-ik_p z}$, results in an FEL interaction at rather long wavelengths. It can sometimes be of interest, but most applications of the relativistic FEL interaction seek shorter wavelengths. Therefore, the backward propagating wave is not discussed here, and we concentrate on waveguide modes with form $E_\perp \propto e^{+ik_p z - i\omega t}$. When the polarization of the waveguide mode is chosen to match the electron motion in the periodic undulator field, we have the best coupling. The form of the transverse electron motion is $\beta_\perp \propto e^{ik_0 z}$ where $\lambda_0 = 2\pi/k_0$ is the undulator wavelength. The fourth component of the Lorentz force equation governs the electron energy evolution and bunching. It has the form $\dot{\gamma} \propto \beta_\perp E_\perp \propto e^{i(k_0+k_p)z - i\omega t}$, and naturally defines the electron phase $\zeta = (k_0+k_p)z - \omega t$ where k_0, k_p, and ω are fixed by the FEL design, and $\zeta(t)$ follows the evolution of $z(t)$. The corresponding the phase velocity is $\propto \dot{\zeta}$. Generally, the electron phase and phase velocity evolve over the whole undulator length L so that it is natural to relate the time t to the evolution time $L/c\,\beta_z \approx L/c$ in the relativistic FEL with electron beam z velocity β_z. The natural definition for the electron phase velocity is then

$$v = L\,[(k_0+k_p)\beta_z - \omega/c\,] = L\left[\left(k_0 + \left[\frac{\omega^2}{c^2} - \Lambda_p^2\right]^{1/2}\right)\beta_z - \frac{\omega}{c}\right] \quad .$$

The electron phase velocity $v(t)$ depends on k_0, k_p, ω, and L, which are fixed in an FEL design, and follows the evolution of the electron z velocity $\beta_z(t)$.

The electron motion in the periodic undulator and interaction with the waveguide mode are resonant when $v = 0$. This occurs at the resonant frequency $\omega^* = c\,(k_0+k_p)\beta_z$ where $k_p = (\omega^{*2}/c^2 - \Lambda_p^2)^{1/2}$. This can solved for ω^* in terms of k_0, k_p, and β_z. The

eigenvalue Λ_p depends on the waveguide dimension and shape. For the rectangular waveguide with sides a and b we have

$$\Lambda_{mn} = \pi \left[\frac{m^2}{a^2} + \frac{n^2}{b^2} \right]^{1/2} ,$$

where $m,n = 0,1,2,3,....$, but not both $m = n = 0$. For the circular waveguide with radius a,

$$\Lambda_{nm} = x_{nm}/a ,$$

where x_{nm} is the root of $J_n'(x_{nm}) = 0$. Looking at the first few roots, we see that roughly, $x_{nm} \approx \pi m$. For both waveguides, the cut-off frequency is $\omega_p = c\Lambda_p$. The NRL waveguide is circular with $a = 1.5$cm so that the lowest values are roughly $\Lambda_p \sim \pi m/a$ and give the cut-off frequency $\omega_p \approx c\pi m/a \approx 10$GHz. The NRL FEL operates above cut-off at $\omega = 35$GHz. Far above cut-off, the expression for the electron phase velocity can be expanded in Λ_p. This give the lowest order shift in phase velocity and clarifies the effect of the waveguide and the FEL performance.

Expanding in Λ_p gives the form of the phase velocity $v = v^{(0)} + \Delta v_p + ...$ where $v^{(0)}$ is the old phase velocity definition without waveguide corrections, $v^{(0)} = L[(k_0+\omega/c)\beta_z - \omega/c]$, and Δv_p is the first order waveguide correction in Λ_p. The old, unperturbed resonance condition, $v^{(0)} = 0$ gives the resonant frequency $\omega^* = ck_0/(1-\beta_z) \approx 2\gamma^2 ck_0/(1+K^2)$. A relativistic FEL that is near resonance $\omega \sim \omega^*$ for maximum coupling, has a shift in phase velocities caused by the waveguide,

$$\Delta v_p \approx - \frac{N \lambda_0^2 \Lambda_p^2 (1+K^2)}{8\pi\gamma^2}$$

where $N = L/\lambda_0$ is the number of undulator periods. The shift in resonance is negative, and diminishes when $\gamma \to \infty$. In a rectangular waveguide

$$\Delta\nu_p^R \approx -\frac{\pi N \lambda_0^2 (1+K^2)}{8\gamma^2}\left[\frac{m^2}{a^2}+\frac{n^2}{b^2}\right] \quad .$$

As an example, consider the LLNL ELF experiment where $\gamma \approx 7$, $\lambda_0 \approx 10$cm, $N \approx 30$, $K \approx 2.4$, and waveguide dimension is $b = 3$cm. The waveguide shift is then $\Delta\nu_{0n}^{ELF} \approx -6\pi n^2$, and $\Delta\nu_{01}^{ELF} \approx -6\pi$ for the lowest order mode. This is a relatively large shift should be detectable. The gain spectrum bandwidth for ELF is $4j^{1/6} \approx 4\pi$ is comparable.

The NRL FEL uses a circular waveguide; the waveguide shift in a circular waveguide is

$$\Delta\nu_p^C \approx -\frac{N \lambda_0^2 (1+K^2)}{8\pi\gamma^2}\left[\frac{x_{nm}}{a}\right]^2 \quad .$$

For the NRL parameters $\gamma \approx 2.4$, $\lambda_0 \approx 4$cm, $N \approx 22$, and $a = 1.5$cm, the shift is $\Delta_{0m}^{NRL} \approx -\pi m^2/2$, and $\Delta_{01}^{NRL} \approx -\pi/2$ in the lowest order mode. The gain spectrum bandwidth is $4j^{1/6} \approx 2\pi$ so that several modes could be near resonance with good coupling.

Gain Degradation and Electron Beam Quality (Summary of Appendix A)

Maintaining the coherence of the electron bunches over a significant interaction length imposes important restrictions on the electron-beam quality. An energy or angular spread (due to emittance) in the NRL experiment would contribute a random component to the electron motion that decreases the coherent bunching in time. Accelerators present a design trade off between high-current and high-beam quality that makes it essential to accurately evaluate the effects of beam quality in present and future experiments. The theoretical approach presented in the publication of Appendix A uses a convenient, yet powerful, method of including an arbitrary electron distribution

function in a self-consistent integral equation for the complex optical field. The FEL is described by solving the Lorentz-Maxwell equations self-consistently in weak optical fields. The field evolution is determined by an integral equation that allows the inclusion of an arbitrary electron distribution function in a simple way. FEL gain and the effects of beam quality can then be calculated analytically or integrated on a small computer. In strong optical fields, the effects of beam quality are diminished because large optical buckets induce and even larger spread than in the initial beam.

Computer simulations are not as useful in solving this kind of FEL problem because they use a prohibitively large number of sample particles, and introduce a large amount of numerical noise when distributed over a large volume of phase space.

In Appendix A, contour maps are used to show the gain degradation due to an electron-beam energy spread and an electron-beam angular spread. Figures 3 and 4 are specifically chosen to represent the NRL experiment. They show that the amount of beam spread expected in the NRL experiment can diminish gain. Furthermore, the two distributions give quite different results for the same amount of spread emphasizing the importance of the detailed shape of the distribution function. When there is high gain, as in the NRL experiment, the exponential growth-rate becomes less susceptible to degradation from the electron-beam quality. Other types of distribution functions can be added to the theoretical technique developed. If solved numerically, even experimental distribution functions peculiar to a given accelerator or transport system can be added.

This research resulted in the publication included in Appendix A. The reference is W. B. Colson, J. C. Gallardo, and P. M. Bosco, "Free-Electron Laser Gain Degradation and Electron Beam Quality", Physical Review A34, 4875 (1986).

Electron Trapping in FEL Oscillators and Amplifiers (Summary of Appendix B)

In high-power FELs, the electrons can become trapped in deep potential wells formed by the combined optical and undulator field forces. The trapped current oscillates at the synchrotron frequency, and can drive the optical wave at sideband frequencies around the fundamental. This "trapped-particle instability" can occur in both the oscillator and amplifier configurations. This is an undesirable effect for many applications, and would certainly be a serious problem for the two-stage FEL.

The trapped-particle instability starts when electrons become trapped in deep potential wells formed by the combined optical and undulator fields. Electrons near the bottom of the well oscillate in harmonic orbits at the synchrotron frequency causing the carrier wave to develop sidebands. The instability has been clearly observed in the high-power FEL oscillator at LANL, and possibly in the TRW/Stanford oscillator. Here, the multimode sideband theory is reviewed with examples from oscillators, and amplifiers. Common features and differences are discussed along with there relevance to the NRL experiment.

Increasing the current density j or the resonator Q increases the steady-state power, the synchrotron frequency, and the sideband gain. Over many hundreds of passes, the stored optical wave "sees" many synchrotron oscillations, so that any sideband gain above threshold gives large growth from a small amount of noise. The resulting steady-state features are therefore not affected by the details of the noise source employed. The addition of sideband power is cumulative, since the presence of a strong sideband again increases the steady-state power. This gives a broad, possibly chaotic, optical power spectrum, and a broad electron distribution. If taper is introduce into the undulator design, the synchrotron frequency is only slightly modified, and the sideband gain is reduced.

If the electron pulse is not short, it is prudent to simulate the FEL by sampling a smaller window with periodic boundary conditions. In the long-pulse limit, as in the NRL

experiment, the wrapped-window approach is the only viable solution to the FEL multimode simulation.

In the high-current FEL amplifier, $j>>1$, large optical power can be produced in a single pass through the undulator. The FEL growth rates are so large that electrons become trapped early in the undulator and begin executing synchrotron oscillations. Even the limited number of synchrotron cycles can result in significant sideband gain owing to the large current density j. The trapped-particle instability in FEL amplifiers differs in many ways from the oscillator case. Sources of noise are much more important, and there is no resonator Q to consider. When the sideband instability does occur, the FEL does not reach steady-state operation even in strong optical fields. The power continues to increase and so does the synchrotron frequency.

This research resulted in the publication included in Appendix B. The reference is W.B. Colson, "The Effect of Electron Trapping in Free-Electron Laser Oscillators and Amplifiers", Proceedings of the 1985 International Conf. on LASERs, Las Vegas CA (1986).

NRL FEL Simulations

Some simlulations are shown below that correspond to the parameters of the NRL FEL experiment. In the next figures, the current density $j = 100$ is used with $Q = 2$ and $Q = 3$. Details of the figures are explained in Appendix B. The evolution of the optical field, optical spectrum, electron spectrum, net gain G, and power are shown. Each simulations starts from shot noise and runs for $n = 200$ passes. Both cases show that the sideband instability has increased the optical spectrum $P(\nu)$ beyond the gain spectrum bandwidth in weak fields $G(\nu)$. When the Q is increased, the power increases, but the spectral quality decreases. The field amplitude $|a(z,n)|$ shown in the upper left corner would provide the electromagnetic undulator in the two-stage NRL FEL. Because of the sideband instability, it would be a poor quality undulator.

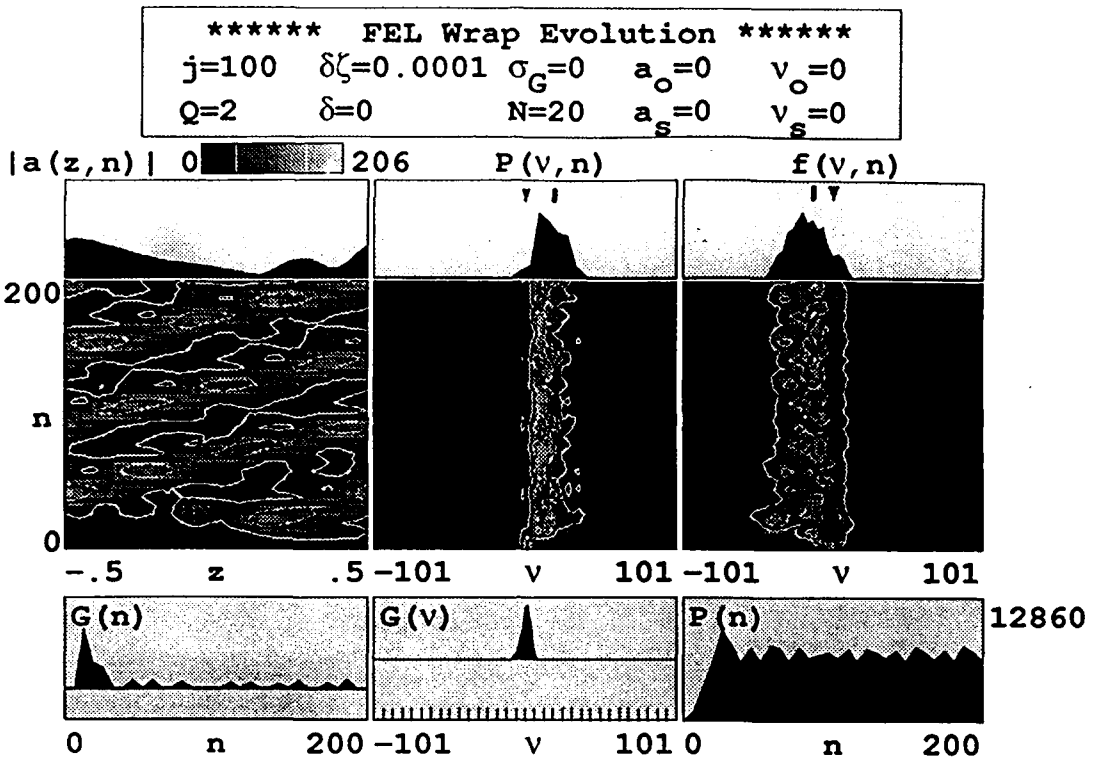
****** FEL Wrap Evolution ******
j=100 δζ=0.0001 σG=0 ao=0 νo=0
Q=2 δ=0 N=20 as=0 νs=0
|a(z,n)| 0 206
P(ν,n)
f(ν,n)
200
n
0
-.5 z .5
-101 ν 101
-101 ν 101
G(n)
G(ν)
P(n)
12860
0 n 200
-101 ν 101
0 n 200

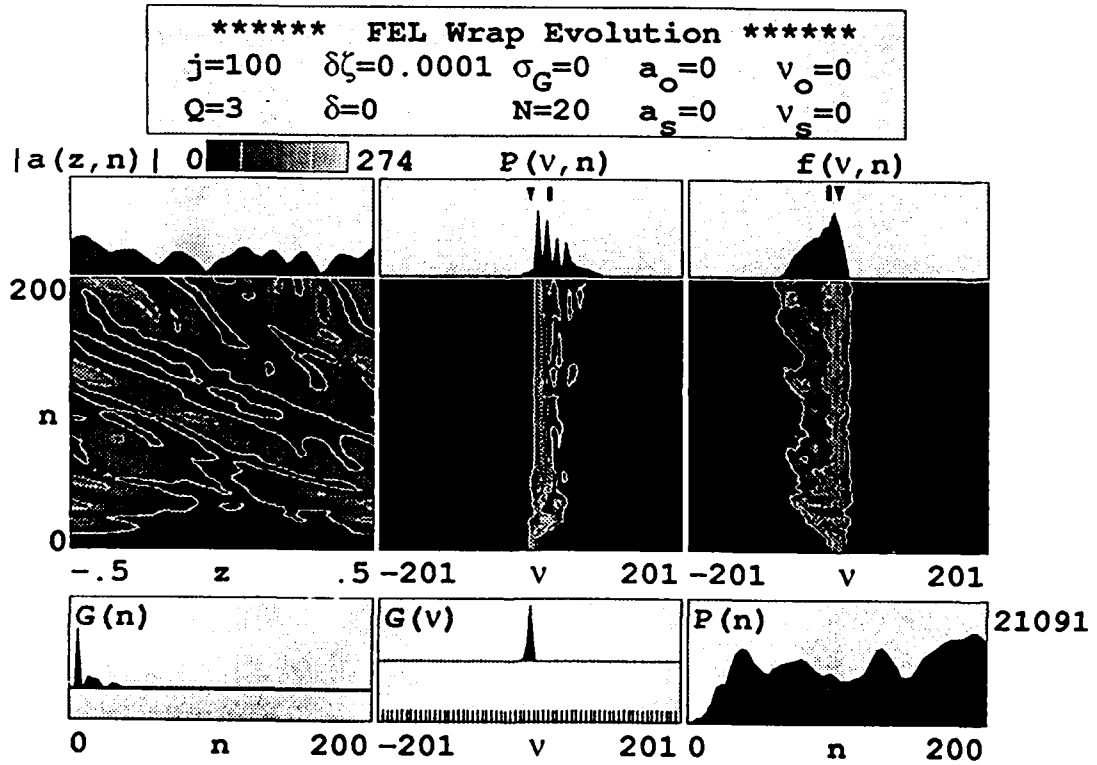
****** FEL Wrap Evolution ******
j=100 δζ=0.0001 σG=0 ao=0 νo=0
Q=3 δ=0 N=20 as=0 νs=0
|a(z,n)| 0 274
P(ν,n)
f(ν,n)
200
n
0
-.5 z .5
-201 ν 201
-201 ν 201
G(n)
G(ν)
P(n)
21091
0 n 200
-201 ν 201
0 n 200

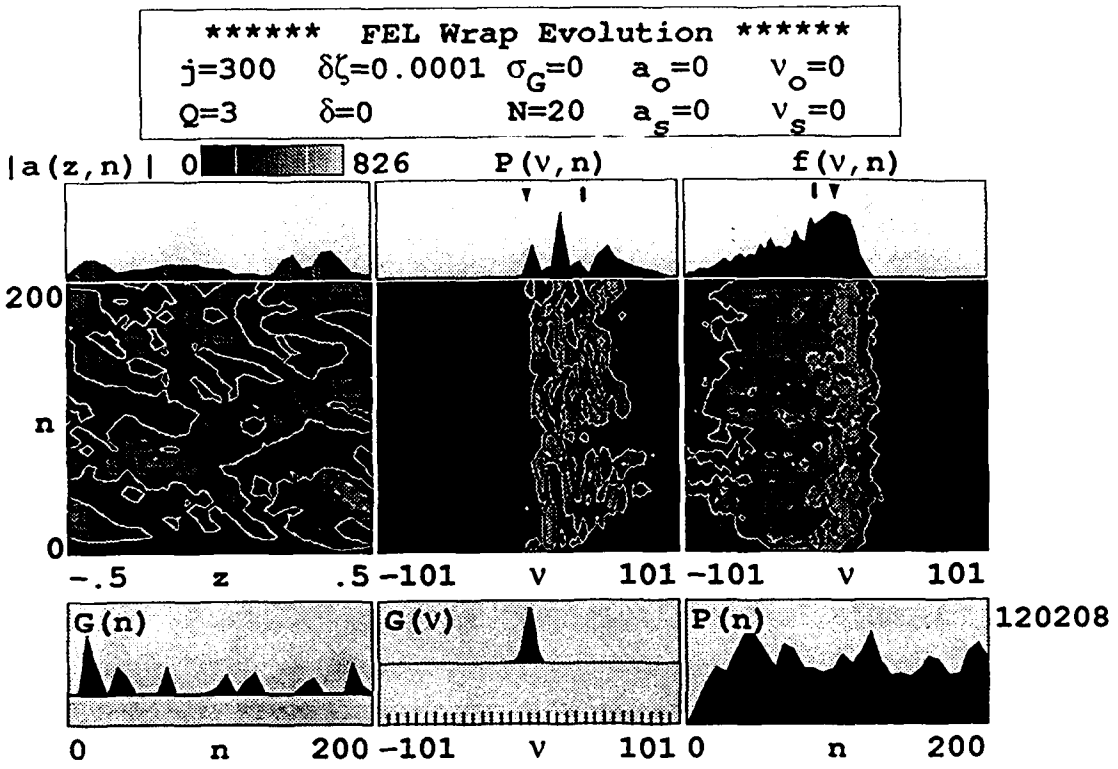
****** FEL Wrap Evolution ******
j=300 δζ=0.0001 σG=0 ao=0 νo=0
Q=3 δ=0 N=20 as=0 νs=0
|a(z,n)| 0 826
P(ν,n)
f(ν,n)
200
n
0
-.5 z .5
-101 ν 101
-101 ν 101
G(n)
G(ν)
P(n)
120208
0 n 200
-101 ν 101
0 n 200

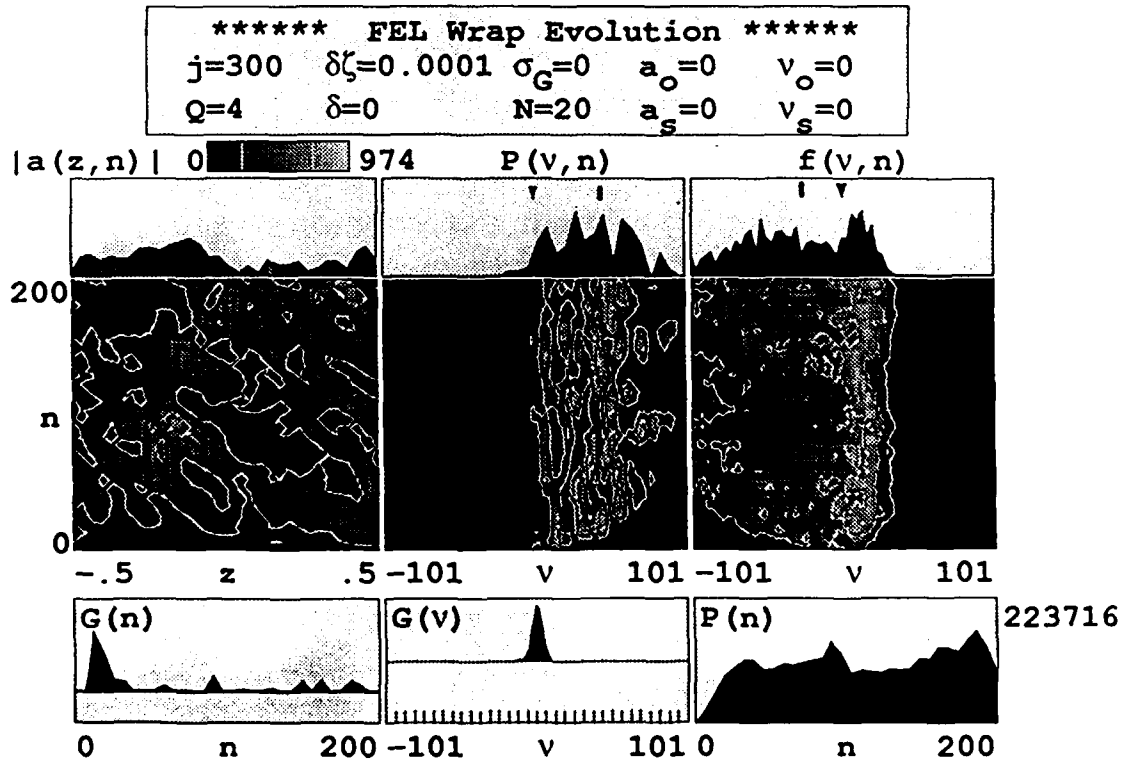
****** FEL Wrap Evolution ******
j=300 δζ=0.0001 σG=0 ao=0 νo=0
Q=4 δ=0 N=20 as=0 νs=0
|a(z,n)| 0 974
P(ν,n)
f(ν,n)
200
n
0
-.5 z .5
-101 ν 101
-101 ν 101
G(n)
G(ν)
P(n)
223716
0 n 200
-101 ν 101
0 n 200

On the previous page the figures show simulation results with the current density $j = 300$ using $Q = 3$ and $Q = 4$. The simulations are started from shot noise and run for 200 passes as in the first two figures. The increased current increases the final field strength dramatically from about $|a| \sim 250$ to $|a| \sim 900$. The increased power spreads the electrons over a wider range of phase velocities, but also degrades the optical spectrum $P(\nu)$. The optical field and spectrum are now chaotic and broad band.

References

[1] C. W. Roberson, J. A. Pasour, F. Mako, R. Lucey, and P. Sprangle, "A Free Electron Laser Driven by a Long Pulse Induction Linac", NRL Memorandum Report 5013 (1983).

[2] J. A. Pasour, R. F. Lucey, and C. A. Kapetanakos, "Long-Pulse, High-Power Free-Electron Laser with No External Beam Focusing", Phys. Rev. Lett. **53**, 1728 (1984).

[3] J. A. Pasour, R. F. Lucey, and C. W. Roberson, "Long Pulse Free Electron Laser Driven by a Linear Induction Accelerator", Free Electron Generators of Coherent Radiation, eds. C. A. Brau, S. F. Jacobs, and M. O. Scully, SPIE vol. **453**, 328 (1984).

[4] J. A. Pasour, and S. H. Gold, "Free-Electron Laser Experiments With and Without a Guide Magnetic Field: A Review of Millimeter-Wave Free-Electron Laser Research at the Naval Research Laboratory," IEEE Journal of Quantum Electronics, Vol. **QE-21**, 845 (1985).

[5]. J. Mathew, and J. A. Pasour, "High-Gain, Long-Pulse Free Electron-Laser Oscillator," Phys. Rev. Lett. **56**, 1805 (1986).

[6] W. P. Marable, P. Sprangle, and Cha-Mei Tang, "High Gain Free Electron Laser Oscillators," NRL Memorandum Report # 5679, (June 6, 1986).

APPENDIX A

Phys. Rev. A34, 4875 (1986).

Free-Electron Laser Gain Degradation and Electron Beam Quality

W. B. Colson

Berkeley Research Associates, P.O. Box 241, Berkeley, CA 94701

J. C. Gallardo and P. M. Bosco

Quantum Institute, University of California, Santa Barbara, CA 93106

ABSTRACT

The free electron laser can be described by solving the Lorentz-Maxwell equations self-consistently in weak optical fields. The field evolution is determined by an integral equation that allows the inclusion of an arbitrary electron distribution function in a simple way. Contour maps are used to show the gain degradation due to an electron beam energy spread and an electron beam angular spread. In the limit of low gain, the gain spectrum is related to the spontaneous emission line-shape through successively higher derivatives. In the limit of high gain, it is shown that the growth rate becomes less susceptible to degradation from the electron beam quality.

I. Introduction

In a free-electron laser (FEL), a relativistic electron beam amplifies a co-propagating, coherent optical wave traveling through a periodic undulator magnetic field [1]. In the oscillator configuration, coherent electron bunching develops on each pass while resonator mirrors allow the stored optical power to grow over many passes. In the amplifier configuration, coherent electron bunches develop rapidly in the first part of the undulator followed by rapid growth of the optical field. Maintaining the coherence of the electron bunches over a significant interaction length imposes important restrictions on the electron beam quality. An energy or angular spread (due to emittance) contributes a random component to the electron motion that decreases the coherent bunching in time.

Some of the earliest FEL experiments used electron beams that were essentially monoenergetic [2-5], but practically all subsequent experiments have made use of higher current sources with significant energy spread or emittance. Many accelerators present a design trade-off between high current and high beam quality. This makes it essential to accurately evaluate the effects of beam quality in present and future experiments. It is particularly important for FELs designed to operate at XUV or X-ray wavelengths [6]. Several theoretical models involving simulations and plasma dispersion relations have discussed the detrimental effects of electron beam quality in the FEL interaction [7-24]. The theory presented here uses a convenient, yet powerful, method of including an arbitrary electron distribution function in a self-consistent integral equation for the complex optical field. FEL gain and the effects of beam quality can then be calculated analytically or integrated on a small computer.

Since the basic equations solved here are the same as in computer simulations or the plasma dispersion methods, specific physical results have been shown to agree with those methods when a direct comparison is possible. The computer simulations have proved to be a useful method of understanding many aspects of the FEL interaction, but one of the most difficult effects to accurately characterize is that of electron beam quality. Even a prohibitively large number of sample particles is far short of the number in a real experiment, and yet introduces a large amount of numerical noise when distributed over a large volume of phase-space. To reproduce some of the results shown later in this paper, we found the simulation method to be several hundred to a thousand times less efficient. While many other FEL topics are most efficiently studied through simulations, the detrimental effects of beam quality are probably better handled through a combination of analytic and numerical techniques. The stability analysis used to obtain plasma dispersion relations usually calculates the reduced FEL growth rates due to poor beam quality. This method can lead to analytical expressions, but depends upon specific models for the electron beam distribution, and does not easily describe more complicated transient behavior where the FEL growth rate is not constant; the FEL is often designed to operate in this regime. In addition, the exact formulation presented here works smoothly between different regimes of operation like high and low gain. The only requirement is weak optical fields.

II. Basic Theory

We solve the electron Lorentz and optical wave equations self-consistently with the assumption of weak optical fields. The effects of beam quality are typically less important when the optical field strength is large near saturation, and the issue of beam quality is most important in weak fields where the accurate evaluation of gain can determine whether the FEL is above or below threshold.

The electrons travel through a periodic undulator with the field on the z-axis described by $\vec{B} = B\ [\cos(k_0 z), \sin(k_0 z), 0]$ where B is the peak magnetic field amplitude. The undulator field extends over a length $L = N\lambda_0$ with a number of periods N, and wavelength $\lambda_0 = 2\pi/k_0$. The electron velocity in a perfect helical orbit is $c\vec{\beta} = c\ [-(K/\gamma)\cos(k_0 z), -(K/\gamma)\sin(k_0 z), \beta_0]$ where $K = eB\lambda_0/2\pi mc^2$, e is the electron's charge magnitude, m is the electron's mass, c is the speed of light, $\beta_0 = (1-(1+K^2)/\gamma^2)^{1/2}$, and γmc^2 is the electron's energy. Imperfect injection due to poor beam quality is more meaningfully introduced after some further theoretical development. A typical undulator uses $B \approx 2$kG and $\lambda_0 \approx 5$cm, so that $K \approx 1$. Since the electrons are relativistic ($\gamma \gg 1$), the transverse excursions are small compared to λ_0.

The optical vector potential with the polarization that best couples to the above trajectory is $\vec{A} = k^{-1}|E|[\sin\psi, \cos\psi, 0]$ where $\psi = kz - \omega t + \phi$, and $\lambda = 2\pi/k = 2\pi c/\omega$ is the optical carrier wavelength. The complex electric field envelope, $E(z,t) = |E(z,t)|e^{i\phi(z,t)}$, is taken to vary slowly in z and t, so that terms containing two derivatives in the wave equation are small compared to terms with single derivative [25]. No transverse (x,y)-dependence is included so that diffraction is taken to be a small over the interaction length L, and the electron beam remains aligned near the center of the optical mode. The transverse motion above, proportional to (K/γ), defines the transverse current for each electron in the beam. If the current density is uniform over a sufficient length, each point $z + ct$ in the optical field envelope evolves according to the slowly-varying wave equation [25]

$$\frac{da}{d\tau} = -j\langle e^{-i\zeta}\rangle \quad , \tag{1}$$

where $a = 4N\pi eKLE/\gamma^2 mc^2$ is the dimensionless optical field strength, $\tau = ct/L$ is the dimensionless time ($0 \le \tau \le 1$), $j = 8N(\pi eKL)^2\rho/\gamma^3 mc^2$ is the dimensionless current density, ρ is the actual electron particle density, $\zeta = (k+k_0)z - \omega t$ is the electron phase in the combined optical and undulator fields, and $\langle\ldots\rangle$ represents a normalized average over all electrons in the beam

driving $a(\tau)$. The electrons are labeled by their initial phase-space coordinates; the initial phase is $\zeta_i = \zeta(0)$, and the initial phase velocity is $\nu_i = d\zeta(0)/d\tau = L[(k + k_0)\beta_0 - k]$. There are a large number of electrons spread randomly over each optical wavelength ($\sim 10^7$), so that the ζ_i can be accurately taken to be uniformly spread along each section of the electron beam one wavelength of light long. It can be easily seen in (1) that bunching the electrons near the relative phase $\zeta + \phi \approx \pi$ drives the optical wave amplitude producing gain, while bunching near $\zeta + \phi \approx \pi/2$ drives the optical phase ϕ without gain. Bunching electrons near $\zeta + \phi \approx 0$ results in negative gain, or absorption. The dimensionless electron phase velocity ν_i has an initial spread associated with the beam quality.

The electron motion in the presence of the optical wave is described by the Lorentz force equation; $d\gamma/dt = -(e/mc)\vec{\beta}\cdot\vec{E}$. In the FEL, it is important to distinguish between collective Coulomb forces and collective high-gain effects [26]. Most FELs do not use current densities large enough for Coulomb forces to be a significant effect for the relativistic electrons; yet, high gain is possible and will be included. Using the definitions and assumptions above, the Lorentz force takes on the form of the pendulum equation [27],

$$\frac{d^2\zeta}{d\tau^2} = \frac{d\nu}{d\tau} = |a|\cos(\zeta + \phi) \quad . \tag{2}$$

The combined equations (1) and (2) are valid in weak or strong optical fields, for large or small gain, and for an arbitrary electron distribution. Strong fields near saturation mean that $|a| \gg \pi$, and weak fields occur when $|a| \ll \pi$. High gain is achieved when $j \gg 1$ and low gain occurs when $j \leq 1$ [28]. Useful FEL configurations display a wide range of current densities. The electron beam area is typically between 1mm and 5mm, but the current ranges from 1A up to 10kA. Undulator lengths L now range from 1m to 5m, but will soon be made to $L = 20$m and beyond. With electron energies in the range 10MeV to 1GeV, the corresponding values of j are from unity to more than 5×10^4 [1]. Both the high-gain, single-pass and the low-gain, oscillator configurations have important applications.

Equations (1) and (2) were originally derived [25] for the more general case where the electron energy can change significantly during a single pass; in this case, an additional factor $\eta = (1 - \nu/2\pi N)$ alters the wave and electron equations so that $\dot{a} = -j < \sqrt{\eta}\, e^{-i\zeta} >$ and, $\ddot{\zeta} = \dot{\nu} = |a|\eta^2\cos(\zeta + \phi)$ with $\dot{(\,)} = d(\,)/d\tau$. The following work, however, will be confined to weak optical fields where $\eta \approx 1$. An extension to higher harmonics and linearly polarized undulators is

also possible without any change in form of (1) and (2), so that the general conclusions and methods of this paper are immediately applicable to a wide range of FEL designs.

We now proceed to solve (1) and (2) in weak fields, $|a| \ll \pi$, to obtain an integral equation for $a(\tau)$ incorporating an arbitrary electron distribution function. The electron phase can be expressed as $\zeta = \zeta_i + \nu_i \tau + \zeta^{(1)}$ where $\zeta^{(1)}$ is the first-order perturbation in a. Expanding (1) and (2) we have

$$a(\tau) = a_0 + ij \int_0^\tau ds < \exp[-i(\zeta_i + \nu_i s)] \zeta^{(1)}(s) > \quad , \tag{3}$$

$$\zeta^{(1)}(s) = \frac{1}{2} \int_0^s dq \int_0^q du [a(u) \exp(i(\zeta_i + \nu_i u)) + a^*(u) \exp(-i(\zeta_i + \nu_i u))] \quad ,$$

where the initial optical field is $a(0) = |a(0)| = a_0$ and $\phi(0) = 0$. We have made use of $< \exp(-i\zeta_i) > = \int_0^{2\pi} d\zeta_i \exp(-i\zeta_i)/2\pi = 0$, since the initial electrons are spread uniformly in phase. The reference to the individual electron phases $\zeta^{(1)}$ can be explicitly removed by combining the equations in (3). Then, we have an integral equation governing the evolution of the optical field $a(\tau)$:

$$a(\tau) = a_0 + \frac{ij}{2} \int_0^\tau ds \int_0^s dq \int_0^q du < \exp(-i\nu_i(s-u)) > a(u) \quad , \tag{4}$$

where <...> is now an average over the initial electron velocity distribution, and all reference to the electron phases has been removed. Since (4) is an iterated triple integral, it may be rewritten [29] as a double integral,

$$a(\tau) = a_0 + \frac{ij}{2} \int_0^\tau ds \int_0^s dq < \exp(-i\nu_i(s-q)) > (s-q)\, a(q) \quad . \tag{5}$$

A normalized electron distribution function $f(\nu_i)$ can be used to evaluate the remaining average: $<...> \equiv \int_{-\infty}^{\infty} d\nu_i \, f(\nu_i)(...)$ with $\int_{-\infty}^{\infty} d\nu_i \, f(\nu_i) = 1$.

III. Simple Electron Distributions

We begin by considering two simple examples with perfect beam quality. In the first, we start the FEL on resonance where the electron-optical wave coupling is largest, $f(\nu_i) = \delta(\nu_i)$. The optical wave is most simply determined from (4).

$$a(\tau) = a_0 + \frac{ij}{2}\int_0^{\tau} ds \int_0^{s} dq \int_0^{q} du\ a(u) \qquad (6)$$

The integral equation (6) can also be written in a differential form by taking successive derivatives, $\dddot{a}(\tau) = ija(\tau)/2$. The complete solution uses the form $a(\tau) = \sum_{n=1}^{3} a_n \exp(\alpha_n \tau)$ where the α_n are the three complex roots of the cubic equation $\alpha^3 - ij/2 = 0$, and the coefficients a_n are determined by the initial conditions $a(0) = a_0$, and $\dot{a}(0) = \ddot{a}(0) = 0$ [1]. *The solution for* $a(\tau)$ *is*

$$a(\tau) = \frac{a_0}{3}\left[\exp\left((j/2)^{1/3}(i+\sqrt{3})\,\tau/2\right) + \exp\left((j/2)^{1/3}(i-\sqrt{3})\,\tau/2\right) + \exp\left(-i(j/2)^{1/3}\tau\right)\right] . \quad (7)$$

If the current density is small $j \to 0$, or $\tau \ll 1$, we have the trivial result $a(\tau) = a_0(1+ij\tau^3/12+\ldots)$ *for an FEL starting on resonance. There is no change in the optical amplitude* $|a| = a_0 + \ldots$ to lowest order, and therefore no gain. The optical phase $\phi(\tau)$ increases slowly in proportion to τ^3. The FEL gain is defined as $G(\tau) = (|a(\tau)|^2 - a_0^2)/a_0^2$, and

$$G(\tau) = \frac{1}{9}\left[2\cosh\left((j/2)^{1/3}\sqrt{3}\,\tau\right) + 4\cos\left((j/2)^{1/3}3\,\tau/2\right)\cosh\left((j/2)^{1/3}\sqrt{3}\,\tau/2\right) - 6\right] . \quad (8)$$

In the high current limit, $j \gg 1$ on resonance, the expressions simplify because one fastest-growing root dominates and describes exponential growth in τ. As seen from (7) there is little change in the field during the bunching time, $\tau < \tau_B \simeq (2/j)^{1/3}$, that precedes exponential growth. During this time, the electrons move from their initially uniform phase distribution to bunch near the phase $\zeta + \phi = \pi/2$. As soon as bunching forms, the high current *immediately causes* exponential field growth and high gain. Then,

$$a(\tau) \simeq \frac{a_0}{3}\exp\left[(j/2)^{1/3}\sqrt{3}\,\tau/2\right] , \quad \text{and} \quad G(\tau) \simeq \frac{1}{9}\exp\left[(j/2)^{1/3}\sqrt{3}\,\tau\right] . \qquad (9)$$

A second simple example is a high quality electron beam starting off resonance at ν_0. This is characterized by $f(\nu_i) = \delta(\nu_i - \nu_0)$. The optical field is then determined by

$$a(\tau) = a_0 + \frac{ij}{2}\int_0^{\tau} ds \int_0^{s} dq \int_0^{q} du\ e^{-i\nu_0(s-u)}\, a(u) . \qquad (10)$$

For low current, $j \leq 1$, *the optical field evolution away from* a_0 *is small so that* $a(u) \simeq a_0$ can can be extracted from the integrand in (10). The resulting integrals are easily solved to obtained the

usual low current gain and phase shift formulas [27].

$$G(\tau) = j\,\frac{2 - 2\cos(\nu_0\tau) - \nu_0\tau\sin(\nu_0\tau)}{\nu_0^3} \quad , \quad \text{and} \quad \phi(\tau) = j\,\frac{2\sin(\nu_0\tau) - \nu_0\tau\,(\,1 + \cos(\nu_0\tau)\,)}{2\nu_0^3} \qquad (11)$$

The maximum final gain is $G = 0.135j$ at $\nu_0 = 2.6$ and $\tau = 1$, while the range of modes with significant gain is $\delta\nu_0 \approx 1$ about the peak.

In order to obtain the general solution, use the substitution $b = a\,e^{i\nu_0\tau}$ in (10). Successive derivatives then lead to the differential form of (10), $\dddot{b} - i\nu_0\ddot{b} - ijb/2 = 0$. Solutions of the form $b = \sum_{n=1}^{3} b_n \exp(\,\alpha_n\tau\,)$ have roots α_n that satisfy the cubic equation $\alpha_n^3 - i\nu_0\alpha_n^2 - ij/2 = 0$. In the limit of high current $j \gg 1$, the exponential gain coefficient is reduced by the factor $-\nu_0^2 / 3\sqrt{3}\,(\,j/2\,)^{1/3}$ so that the gain spectrum is centered about $\nu_0 = 0$ with a characteristic range $\delta\nu_0 \approx 4.22j^{1/6}$. In the high current case, the range of modes with significant gain increases slowly as j increases. We go on now to look at more interesting FEL distributions describing less than perfect electron beams.

IV. More General Electron Distributions

New cases of interest involve more complicated distributions $f(\nu_i)$ describing the initial electron beam in the integral equation (5). Two electrons starting at the same phase ζ_i at the beginning of the undulator ($\tau = 0$), but with different z-velocities, $c\,\beta_0$ and $c\,(\beta_0 + \Delta\beta_0)$, will drift apart as they travel through the undulator. The amount of drift is not easily predicted without solving the full problem, because electrons can influence each other through the self-consistently evolving optical wave. In this sense, the effect of FEL beam quality is collective. However, the times for the two electrons to traverse the undulator are nearly identical since they are relativistic, $L/\beta_0 c \approx L/(\beta_0 + \Delta\beta_0)c \approx L/c$. An estimate of their separation at the end of the undulator ($\tau = 1$) is $\Delta z \approx \Delta\beta_0 L$, and their approximate phase difference is $\Delta\zeta = (k + k_0)\Delta z \approx k\,\Delta z \approx kL\,\Delta\beta_0$. If the velocity difference $\Delta\beta_0$ is due to an initial energy difference $\Delta\gamma mc^2$, we have $\Delta\beta_0 \approx (1+K^2)\Delta\gamma/\gamma^3$, and an approximate final phase separation $\Delta\zeta \approx 4\pi N\,\Delta\gamma/\gamma$.

Any random phase difference $\Delta\zeta \sim \pi$, or larger, between electrons in the beam is important to the FEL operation, because bunching on the optical wavelength scale is diminished significantly. At the end of the undulator, the final phase difference is roughly estimated by $\Delta\zeta \approx \Delta\nu_i$ for each electron. From the definition of the electron phase velocity ν_i, we see that a

small change in the initial electron energy $\Delta\gamma mc^2$ corresponds to a change in the initial phase velocity, $\Delta v_i \approx 4\pi N \Delta\gamma / \gamma$ for $\gamma \gg 1$. A distribution of initial electron energies from an accelerator or storage ring is often accurately represented by the normal distribution function so that we can take

$$f(v_i) = \frac{\exp(-(v_i - v_0)^2 / 2\sigma^2)}{\sqrt{2\pi}\,\sigma} \quad , \tag{12}$$

where σ is the standard deviation of v_i away from the peak phase velocity v_0. If $\Delta\gamma mc^2$ is taken to be the standard deviation of the electron energy away from γmc^2, then $\sigma \approx 4\pi N \Delta\gamma / \gamma$. Two electrons starting at the same phase ζ_i , but with an energy difference $\Delta\gamma = \gamma / 4N$ will drift apart by roughly half of one optical wavelength at the end of the undulator. A random spread of width $\sigma = \pi$ causes a random phase spread of approximately $\Delta\zeta \approx \pi$ at the end of the undulator and impairs bunching. Inserting (12) into (5) gives

$$a(\tau) = a_0 + \frac{ij}{2}\int_0^\tau ds \int_0^s dq\; e^{-\sigma^2(s-q)^2/2}\, e^{-iv_0(s-q)}\,(s-q)\,a(q) \quad . \tag{13}$$

The gaussian factor in the integrand decreases the coupling current j as τ increases, and describes the degradation of bunching due to the spread in electron phase velocities. The complicated self-consistent evolution of the electron beam distribution and the optical field are described exactly in (13), but before evaluation, we can generalize its form further.

An angular spread is also possible due to the finite emittance of an electron beam. An electron of energy γmc^2 entering the undulator with a small injection angle θ_i has a reduced z-velocity, $\beta_0 \rightarrow \beta_0 \cos\vartheta_i \approx \beta_0 (1 - \theta_i^2 / 2)$. The resulting z-velocity change is $\Delta\beta_0 \approx -\theta_i^2 / 2$, reducing the initial phase velocity by $\Delta v_i = -2\pi N \gamma^2 \theta_i^2 / (1+K^2)$. A gaussian distribution of angles about the z-axis with standard deviation $\Delta\theta_i$ gives the exponential distribution function

$$f(v_i) = \frac{\exp(-(v_0 - v_i)/\sigma_\theta)}{\sigma_\theta} \quad \text{for} \quad v_i < v_0 \quad , \text{ and } \quad f(v_i) = 0 \quad \text{for} \quad v_i > v_0 \quad , \tag{14}$$

where $\sigma_\theta = 4\pi N \gamma^2 \Delta\theta_i^{\,2} / (1+K^2)$, and v_0 is the phase velocity for electrons entering on-axis. The distribution function (14) is sharply peaked at $v_i = v_0$ where electrons enter on-axis, and decays exponentially for $v_i < v_0$ because the injection at any angle θ_i can only decrease the electron's longitudinal velocity and its phase velocity v_i. If each element of the energy distribution (12) is given an angular spread according to (14), then the resulting integral equation for the optical field becomes

$$a(\tau) = a_0 + \frac{ij}{2}\int_0^\tau ds \int_0^s dq \; \frac{e^{-\sigma^2(s-q)^2/2}}{1 - i\sigma_\theta(s-q)} \, e^{-iv_0(s-q)} \, (s-q)\, a(q) \quad . \tag{15}$$

The transverse motion of electrons injected at an angle is sometimes confined by either the natural off-axis undulator fields or external focusing elements. The focusing forces result in transverse betatron oscillations about the undulator axis. When the electron beam is injected to match the natural focusing properties of an undulator, the number of betatron oscillations along the undulator is $N_\beta \approx NK/\sqrt{2}\gamma$. In the limit of large γ and/or small K, the angular spread of electrons can be important, $\sigma_\theta > 1$, while the transverse focusing can be made negligible, $N_\beta < 1$. In this limit, the integral equation (15) applies.

The complex optical field $a(\tau)$ now depends on an input energy spread characterized by σ, and an input angular spread characterized by σ_θ. Other types of distribution functions can be added in a similar way. If (5) is solved numerically, even experimental distribution functions peculiar to a given accelerator or transport system can be added. The general result (5) and the specific example (15) are important results of this paper. They provide analytic expressions describing FEL performance with an arbitrary electron distribution function.

V. Low-Current FELs

One of the cases of general interest is the low current FEL oscillator. Radiation energy is stored in an optical resonator, and repeatedly driven by successive electron pulses from an accelerator like a linac or storage ring. An important issue for the oscillator is the detrimental effect of the electron energy and angular distributions when the oscillator is starting from weak optical fields. In the low-current case, we can simplify (15) by taking $a(q) \approx a_0$ in the integrand of the integral equation, and neglecting higher-order terms in j. Without $a(q)$ in the integrand, the integral can be further simplified by noticing that $iqe^{-iv_0 q} = -\partial_{v_0} e^{-iv_0 q}$. Then,

$$\frac{a(\tau) - a_0}{a_0} = -\frac{j}{2}\frac{\partial}{\partial v_0}\int_0^\tau ds \int_0^s dq \; \frac{e^{-\sigma^2 q^2/2}}{1 - i\sigma_\theta q} \, e^{-iv_0 q} \quad . \tag{16}$$

Direct integration of (16) is possible, but the result is a complicated expression containing many error-functions [30].

We can alter the form of (16), however, to obtain some important physical interpretations. The factors $e^{-\sigma^2 q^2/2}$ and $(1 - i\sigma_\theta q)^{-1}$ can be interpreted as power series expansions in q

multiplying the factor $e^{-i\nu_0 q}$; then $(-iq)^n e^{-i\nu_0 q} \rightarrow \partial_{\nu_0}^n e^{-i\nu_0 q}$. Now, write

$$\frac{a(\tau)-a_0}{a_0} = -\frac{j}{2}\frac{\exp(\sigma^2\partial_{\nu_0}^2/2)}{1+\sigma_\theta\partial_{\nu_0}}\partial_{\nu_0}\int_0^\tau ds\int_0^s dq\, e^{-i\nu_0 q} \quad . \tag{17}$$

The double integral is simply $\nu_0^{-2}(1-i\nu_0\tau-e^{-i\nu_0\tau})$, so that the complex integrations in (16) have been replaced with a power series expansion to all orders in σ and σ_θ. To first order in σ and σ_θ, an explicit expression for $a(\tau)$ is easily obtained from (17). This is a useful limiting case since a low-current FEL system would not typically use a low quality electron beam (large σ or σ_θ) and remain above threshold. From (17), the low-current FEL gain at the end of the undulator is

$$G = -\frac{j}{2}\frac{\exp(\sigma^2\partial_{\nu_0}^2/2)}{1+\sigma_\theta\partial_{\nu_0}}\partial_{\nu_0}\left[\frac{\sin^2(\nu_0/2)}{(\nu_0/2)^2}\right] \quad . \tag{18}$$

We recognize the factor in brackets [...] as the FEL spontaneous emission line-shape for an electron in a perfect trajectory through the undulator. It has been known for some time that the gain is fundamentally related to the derivative of the spontaneous emission line-shape [31]. The new feature presented in (18) is to express how the electron beam energy and angular spreads affect that relationship through successively higher derivatives.

With the physical interpretation of the line-shape factor [...] , we can substitute alternate forms. One convenient choice is $[...] \rightarrow \exp(-\nu_0^2/4\pi)$ which approximately reproduces the correct features of the simple FEL gain spectrum, $G \approx (j\nu_0/4\pi)\exp(-\nu_0^2/4\pi)$. The successive derivatives evaluating the effects of beam quality lead to more compact expressions, and illustrate how (18) can be used in practical situations. Even an experimental line-shape could be used in (18).

While the analytic results presented have their merit, the complete integral (15) is easy to integrate on a small computer. The values needed for the contour plots of this paper were evaluated in this way. Figure 1 shows a combined intensity and contour plot of $\ln(1+G(\sigma,\nu_0))$ where the final gain at the end of the FEL undulator is $G = (a^*(1)\,a(1) - a_0^2)/a_0^2$. In Fig. 1 $\sigma_\theta = 0$, so that gain degradation is only due to an energy spread with no angular spread. The current density is $j = 1$, and gives low gain so that $\ln(1+G) \approx G$. The brightest points (white) on the (σ,ν_0)-surface indicate peak gain $G \approx 0.13j$, while the darkest points (black) indicate maximum absorption $G \approx -0.13j$. Zero gain is indicated by the intermediate grey shown in the scale at the

top. Specific contours of constant gain, $\ln(1+G) = \pm 0.06, \pm 0.08, \pm 0.1$, and ± 0.12, are superimposed on the intensity plot. The gain surface is approximately antisymmetric about $v_0 = 0$, and in the limit $j \to 0$, the gain $G(\sigma, v_0)$ becomes exactly antisymmetric. The characteristic amount of spread required to decrease the gain is seen from Fig. 1 and (18) to be $\sigma^* \approx 1$. Note also that as the spread σ increases, the phase velocity for peak gain $v_0^* \approx 2.6$ increases slightly. Peak absorption occurs at $-v_0^*$ and slightly decreases with increasing σ.

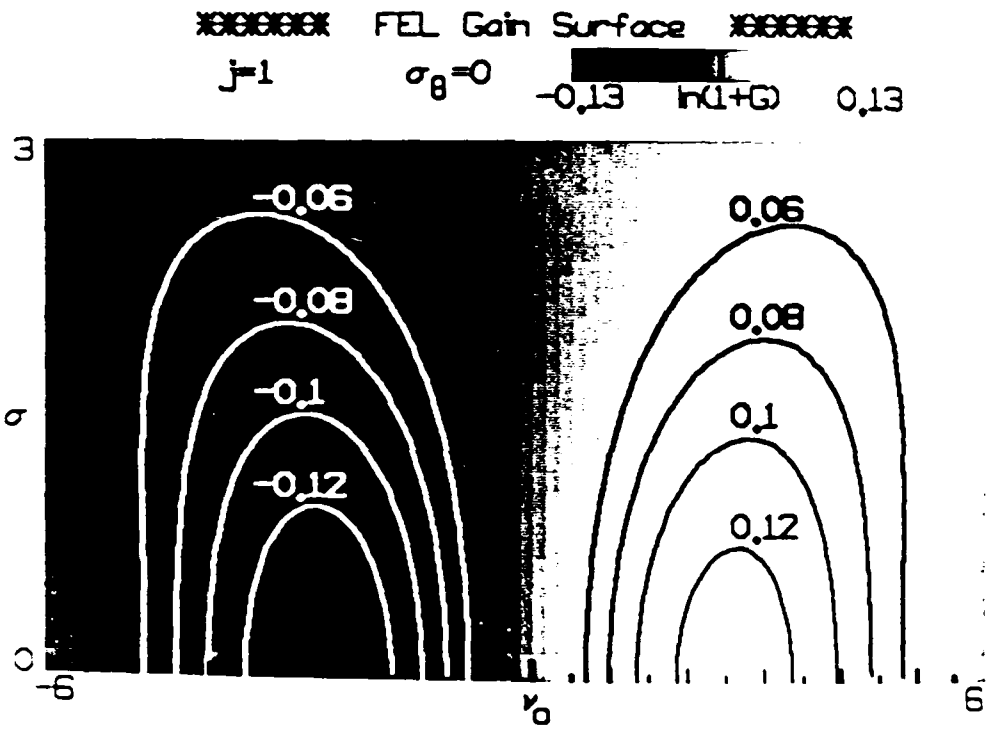

Fig. 1. Intensity and contour plot of $\ln(1+G(\sigma, v_0))$ with $j = 1$ and $\sigma_\theta = 0$. The weak-field gain degradation in this low-current FEL is due to an electron beam energy spread with a normal distribution function.

Figure 2 shows a combined intensity and contour plot of $\ln(1+G(\sigma_\theta, v_0))$ evaluated by (15) with $j = 1$ and $\sigma = 0$. The gain degradation here is due to a monoenergetic electron beam entering the undulator with an angular spread described by σ_θ. The grey scale and contours of gain are the same as in Fig. 1. Unlike Fig. 1, the absorption contours (white) have a much different shape than the gain contours (black). Since the distribution function $f(v_i)$ due to an angular spread is skewed, there is no reason to expect the antisymmetric properties of $G(\sigma_\theta = 0, v_0)$ to be

maintained at $\sigma_\theta > 0$. As seen in Fig. 1 and (18), the characteristic value for the degradation of gain is $\sigma_\theta * \approx 1$. The phase velocity for peak gain, and peak absorption, both increase with increasing σ_θ roughly as $v_0 * \approx \sigma_\theta$. Note that the general features of Figs. 1 and 2 are quite different owing to the different forms of the electron distributions. This emphasizes the importance of the shape of the electron distribution in evaluating gain degradation in FELs, and the need for an accurate, flexible theory as presented here.

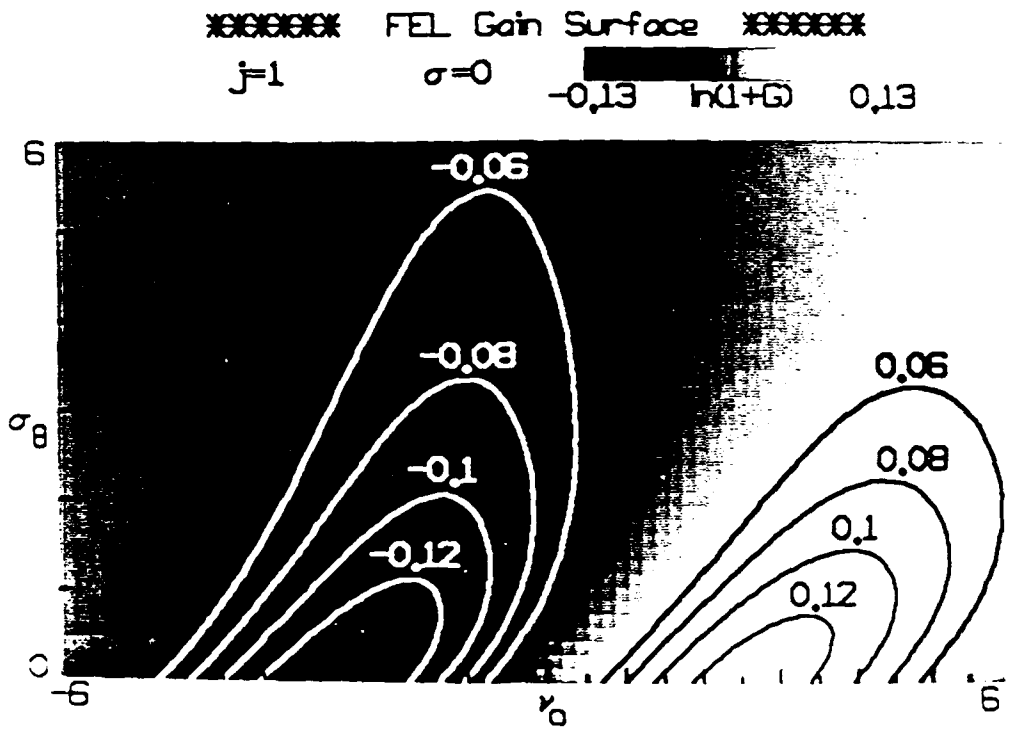

Fig. 2. Intensity and contour plot of $\ln(1+G(\sigma_\theta, v_0))$ with $j = 1$ and $\sigma = 0$. The weak-field gain degradation in this low-current FEL is due to an electron beam angular spread with a normal distribution; the resultant phase-velocity distribution is the exponential distribution function.

VI. High-Current FELs

The integral representation of the optical field in (15) is also valid for high-current FELs where $j \gg 1$. In this case, $a(\tau)$ acquires a non-linear dependence on j (recall expression (7)) and cannot be removed from the integrand of (15). To proceed analytically, it is convenient to remove one integral from (15) by taking the τ-derivative of both sides, and use the form $a = a_0 e^{\alpha \tau}$

for the optical field. Since $j \gg 1$, assume that α has some large real part, even though the exponential growth may be somewhat diminished by the presence of σ and σ_θ. The magnitude a_0 cancels on both sides, and a change of variables gives the form

$$\alpha^3 \approx \frac{ij}{2}\int_0^\infty ds\, s\, e^{-s}\, \frac{e^{-\sigma^2 s^2/2\alpha^2}}{1-i\sigma_\theta s/\alpha}\, e^{-iv_0 s/\alpha} \quad . \tag{19}$$

The upper integration limit in (19) has been extended to infinity because the integrand containing the factor e^{-s} becomes negligible for large s.

Eqn. (19) describes several properties of high-gain FELs without integration. If σ, v_0, and σ_θ all $\to 0$, then α has the same roots found in (7). If the current density $j \to \infty$ so that a real part of $\alpha \to \infty$, then we obtain the same limit, since σ, v_0, and σ_θ all appear divided by α in (19). Unlike the low-current FEL, the importance of beam quality in a high-current FEL depends on the current density j. This feature has been seen in FEL experiments and simulations, but is now expressed analytically. The importance of beam quality can be made more quantitative by iterating (19). Estimating the real part of the fast-growing root as $\alpha^* = (j/2)^{1/3}\sqrt{3}/2$, the integrand of (19) is only significantly modified when $\sigma^* \approx (j/2)^{1/3}\sqrt{3/2}$ or when $\sigma_\theta^* \approx (j/2)^{1/3}\sqrt{3}/2$. In the high-current FEL, the characteristic values of beam quality, σ^* and σ_θ^*, are not equal, and increase with the current density j. These expressions should be helpful in designing high-gain experiments where there is a trade-off between beam quality and beam current.

Figure 3 shows a combined intensity and contour plot of $\ln(1+G(\sigma,v_0))$ for moderately high current $j = 100$ and $\sigma_\theta = 0$. The points at the peak gain $\ln(1+G) = 4.3$ are indicated by white on the (σ,v_0)-surface; black indicates zero gain. Contours of constant gain, $\ln(1+G) = 2.0$, 2.5, 3.0, 3.5, and 4.0 are superimposed on the intensity plot. For the high quality electron beam, small σ, gain is confined to a region near resonance, but extends to a broader range in v_0 than in the low-current cases of Figs. 1 or 2. This agrees with the discussion below (11), and gives the range of optical wavelengths over which there is significant gain $\delta v_0 \approx 4j^{1/6} \approx 7$. To find the range of wavelengths, use $\Delta\lambda/\lambda = \Delta v_0/2\pi N$ about the resonant wavelength $\lambda = \lambda_0(1+K^2)/2\gamma^2$. The maximum available gain decreases significantly as $\sigma \to \sigma^* \approx 4.5$ as predicted in the previous paragraph, and the phase velocity for peak gain roughly follows $v_0^* \approx \sigma$.

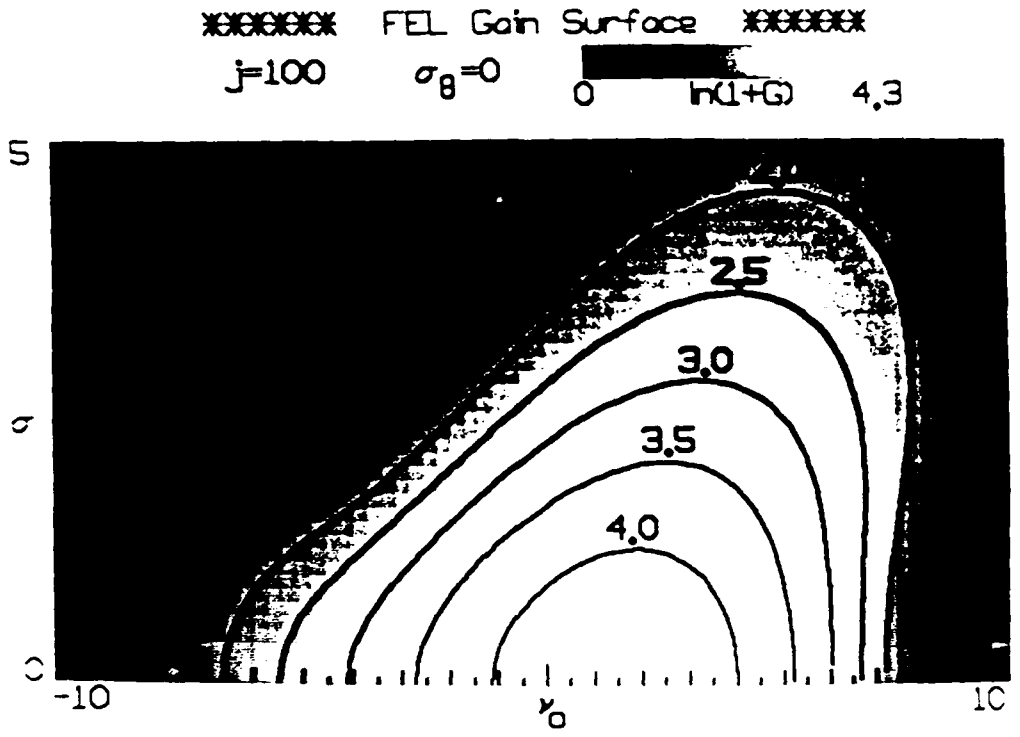

Fig. 3. Intensity and contour plot of $\ln(1+G(\sigma,\nu_0))$ with $j = 100$ and $\sigma_\theta = 0$. The weak-field gain degradation in this FEL is due to an electron beam with a normal distribution in energy.

Figure 4 shows the plot of $\ln(1+G(\sigma_\theta,\nu_0))$ with $\sigma = 0$ so that the gain degradation is caused by an angular spread in the electron beam. The contours of constant gain differ from Fig. 3 because of the new shape of the electron distribution function. As σ_θ increases, there is a slower decrease in gain because $\sigma_\theta^* > \sigma^*$ as found above. When expressed in dimensionless form, an angular spread is better tolerated in an FEL than is an energy spread. The points of peak gain increase with increasing σ_θ similar to Fig. 3.

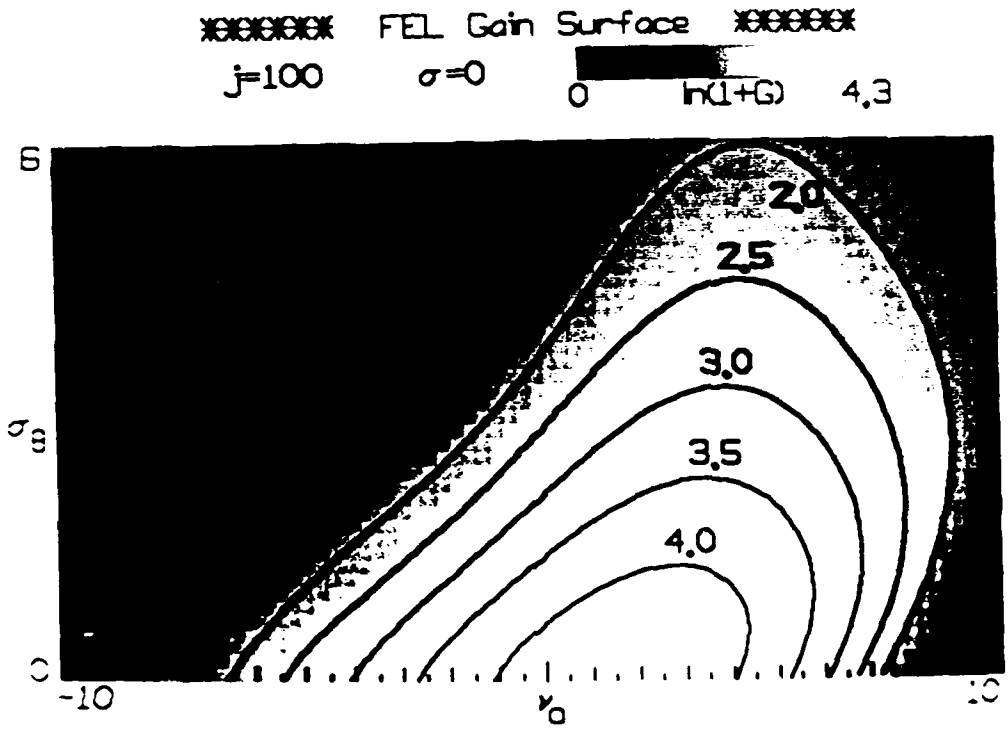

Fig. 4. Intensity and contour plot of $\ln(1+G(\sigma_\theta,\nu_0))$ with $j = 100$ and $\sigma = 0$. The weak-field gain degradation in this FEL is due to an electron beam with an angular spread producing an exponential distribution in phase velocities.

Figure 5 shows the combined intensity and contour plot of $\ln(1+G(\sigma,\nu_0))$ for high current $j = 10^4$ with $\sigma_\theta = 0$. There are no negative gain regions, and the available peak gain is much larger than for the lower current. For $\sigma = 0$, the position of peak gain is essentially at resonance $\nu_0 = 0$, but again increases roughly as $\nu_0^* \approx \sigma$ while beam quality diminishes. The width of the gain spectrum at $\sigma = 0$ is wider than the lower current case, and agrees well with $\delta\nu_0 \approx 4j^{1/6} \approx 12$. The contours of constant gain, $\ln(1+G) = 14, ..., 24$, show that the range of wavelengths for gain becomes narrower as σ increases, and the maximum available gain decreases significantly as $\sigma \rightarrow \sigma^* \approx 20$.

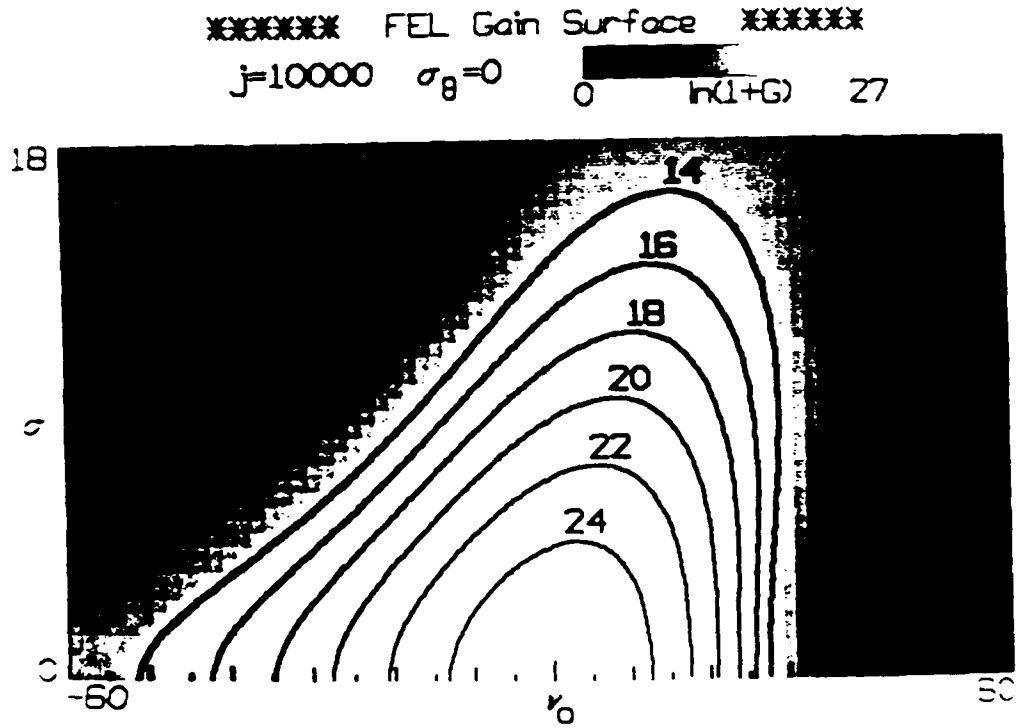

Fig. 5. Intensity and contour plot of $\ln(1+G(\sigma,\nu_0))$ with $j = 10^4$ and $\sigma_\theta = 0$. The weak-field gain degradation in this high-gain FEL is due to an electron beam with a normal distribution in energy.

Figure 6 shows the plot of $\ln(1+G(\sigma_\theta,\nu_0))$ for high current $j = 10^4$ with $\sigma = 0$. Again, the contours of constant gain, $\ln(1+G) = 14, ..., 24$, are distinct from Fig. 5 showing the importance of the electron beam distribution function even at high gain. As $\sigma_\theta \rightarrow \sigma_\theta^*$, the gain decreases significantly, but again the angular spread is seen to be less harmful than an energy spread. Unlike Fig. 5, the position of peak gain stays closer to resonance as σ_θ increases.

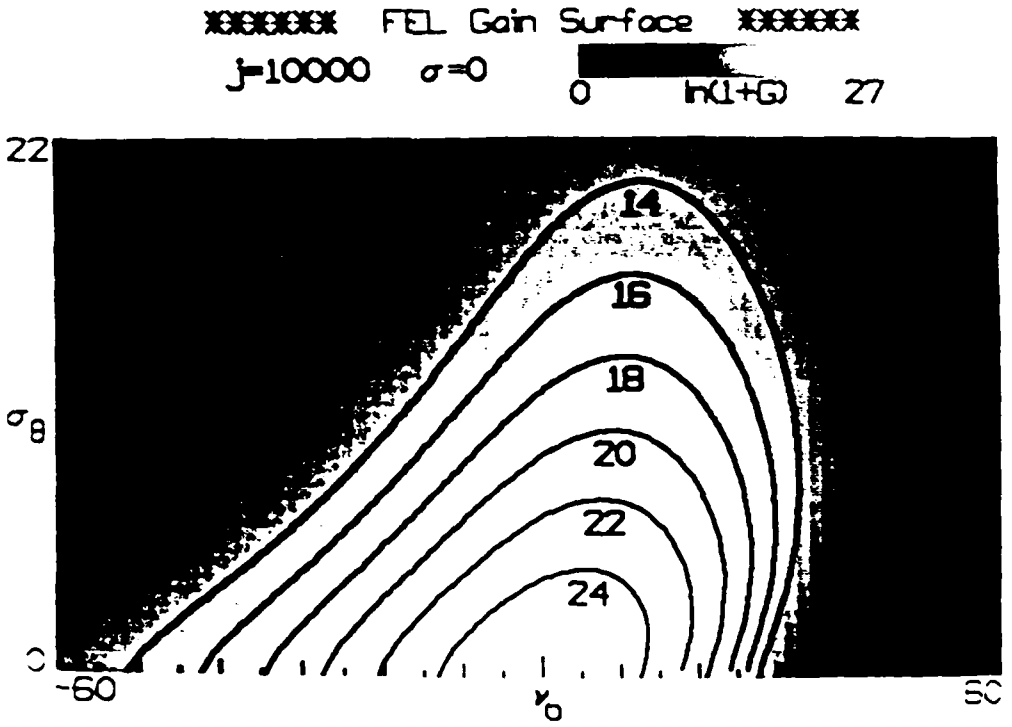

Fig. 6. Intensity and contour plot of $\ln(1+G(\sigma_\theta,\nu_0))$ with $j = 10^4$ and $\sigma = 0$. The weak-field gain degradation in this high-gain FEL is due to an electron beam with an angular spread producing an exponential distribution in phase velocities.

Acknowledgments

The authors are grateful for support of this research by the U.S. Office of Naval Research, the Los Alamos National Laboratory, the Naval Research Laboratory, and the Lawrence Berkeley Lab, and would like to thank S. W. McDonald for helpful discussions.

References

1. W. B. Colson and A. M. Sessler, Annuals Reviews of Nuclear and Particle Science 35, 25 (1985).

2. S. Benson, D. A. G. Deacon, J. N. Eckstein, J. M. J. Madey, K. Robinson, T. I. Smith and R. Taber, J. de Physique **44**, Colloque C1, 353 (1983).

3. J. A. Edighoffer, G. R. Neil, C. E. Hess, T. I. Smith, S. W. Fornaca and H. A. Schwettman, Phys. Rev. Lett. **52**, 344 (1984).

4. Billardon, M. et. al., Phys. Rev. Lett. **51**, 1652 (1983).

5. L. R. Elias, J. Hu, and G. Ramian, Nucl. Instr. and Math. in Phys. Res. **A237**, 203 (1985).

6. *Free-Electron Generators of Extreme Ultraviolet Coherent Radiation*, AIP Conf. Proc. No. **118**, eds. Madey and Pellegrini, Brookhaven National Lab, Upton NY (1984).

7. V. K. Neil, JASON Technical Report JSR-79-10 (l979).

8. Ira B. Bernstein and J. L. Hirshfield, Phys. Rev. Lett. **40**, 761 (1978).

9. Ira B. Bernstein and J. L. Hirshfield, Phys. Rev. **20A**, 1661 (1979).

10. N. M. Kroll and W. A. McMullin, Phys. Rev. **A17**, 300 (1978).

11. P. Sprangle, Cha-Mei Tang, and W. M. Manheimer, Phys. Rev. **A21**, 302 (1980).

12. P. Sprangle and Robert A. Smith, Phys. Rev. **A21**, 293 (1980).

13. W. B. Colson and S. K. Ride, *Physics of Quantum Electronics*, **7**, 377, eds. Jacobs, Pilloff, Sargent, Scully, and Spitzer (Addison-Wesley 1980).

14. F. Ciocci, G. Dattoli and A. Renieri, Lettere Al Nuovo Cimento **34**, 342 (1982).

15. I. Boscolo, M. Leo, R.A. Leo and G. Soliani, Il Nuovo Cimento **2D**, 64 (1983).

16. J. C. Goldstein, W. B. Colson, and R. W. Warren, Bendor Free Electron Laser Conference, J. de Physique **44**, C1-371 (1983).

17. L. F. Ibanez and S. Johnston, IEEE Journal of Quantum Electron. **QE-19**, 339 (1983).

18. J. Gea-Banacloche, G. T. Moore, and M. O. Scully, *Free Electron Generators of Coherent Radiation*, SPIE **453**, 393 (Society of Photo-Optical Inst. Eng. 1983).

19. J. Gea-Banacloche, G. T. Moore, and M. O. Scully, *Free Electron Generation of Extreme Ultraviolent Coherent Radiation*, AIP Conf. Proceedings No. 118, eds. J. M. J. Madey and C. Pellegrini, p. 161 (American Inst. of Physics 1984).

20. G. T. Moore. Opt. Commun. **54**, 121 (1985).

21. L. K. Grover, J. Feinstein, R. H. Pantell, IEEE J. Quant. Electron. **QE-21**, 470 (1985).

22. K.-J. Kim, Seventh Annual Free Electron Laser Conference, Lake Tahoe CA (1985).

23. G. Dattoli and A. Renieri, *Experimental and Theoretical Aspects of the Free Electron Laser*, Laser Handbook, **4**, eds. M. L. Stich and M. S. Bass (North-Holland, Amsterdam, 1985).

24. E. Jerby and A. Gover, IEEE J. Quantum Electron. **QE-21**, 1041 (1985).

25. W. B. Colson and S. K. Ride, Phys. Lett. **76A**, 379 (1980).

26. W. B. Colson, IEEE J. Quantum Electron. **QE-17**, 1417 (1981).

27. W. B. Colson, Phys. Lett. A**64**, 190 (1977).

28. W. B. Colson and R. A. Freedman, Phys. Rev. **A27**, 1399 (1983).

29. M. Abramowitz and I. A. Stegun, Handbook of Mathematical Functions, p. 891, National Bureau of Standards, 1972.

30. P. M. Bosco, Ph.D. Thesis, University of California at Santa Barbara, 1985.

31. J. M. J. Madey, J. Appl. Phys. **42**, 1906 (1971).

APPENDIX B

Proc. Int. Conf. on Lasers '85, STS Press, p. 751 (Sept. 1986).

The Effect of Electron Trapping in Free-Electron Laser Oscillators and Amplifiers

W. B. Colson

Berkeley Research Associates, P.O. Box 241, Berkeley, California 94701

ABSTRACT

In high-power free-electron lasers, the electrons can become trapped in deep potential wells formed by the combined optical and undulator field forces. The trapped current oscillates at the synchrotron frequency, and can drive the optical wave at sideband frequencies around the fundamental. This "trapped-particle instability" can occur in both the oscillator and amplifier configurations.

1. Introduction

Many free-electron laser (FEL) oscillators [1], and FEL amplifiers [2] are designed to produce large optical power. In both configurations, a relativistic, high-current electron beam amplifies a copropagating electromagnetic wave as they pass through a periodic, transverse magnetic field undulator. The trapped-particle instability starts when electrons become trapped in deep potential wells formed by the combined optical and undulator fields. Electrons near the bottom of the well oscillate in harmonic orbits at the synchrotron frequency causing the carrier wave to develop sidebands. The "trapped-particle instability" was first predicted using a single-mode theory describing high-power, low-gain FEL oscillators with a tapered undulator [3]; the tapered undulator design reaches high power by trapping electrons in potential wells that remain resonant as the electrons lose energy [4]. At the same time, multimode simulations of short-pulse FEL oscillators observed the effects of the instability as pulse modulation [5-7]. Recently, the instability has been observed in the high-power FEL oscillator at LANL [1], and possibly in the TRW/Stanford oscillator [8]. It has been termed the sideband, Kroll-Rosenbluth, synchrotron, Raman, and the trapped-particle instability [9-23]. Here, the multimode sideband theory is reviewed with examples from short-pulse FELs, oscillators, and amplifiers. Common features and differences are discussed.

2. Multimode Simulation Theory

The electrons injected into the FEL undulator evolve due to the combined optical and undulator electromagnetic fields. When the relativistic electrons of energy $\gamma_0 mc^2$ ($\gamma_0 >> 1$) are properly injected into the undulator, the transverse electron motion is periodic with amplitude $K\lambda_0/2\pi\gamma_0$ and phase $\exp(ik_0 Z)$ where $K = e\bar{B}\lambda_0/2\pi mc^2$, e is the electron charge magnitude, $\bar{B}$ is the rms undulator field strength, $\lambda_0 = 2\pi/k_0$ is the undulator wavelength, m is the electron mass, and c is the speed of light in vacuum. The average speed of the beam along the Z-axis is $\beta_0 c$ where $\beta_0 \approx 1 - (1+K^2)/2\gamma_0^2$. We follow the beam evolution with the dimensionless time $\tau = \beta_0 ct/L = 0 \rightarrow 1$ along the undulator length $L = N\lambda_0$ with N periods.

The light wave evolves in the presence of the electron beam according to the transverse wave equation. The optical carrier wave with frequency $\omega = kc = 2\pi c/\lambda$ has the single-mode phase $\exp[i(kZ - \omega t)]$ and a complex slowly-varying coefficient $a(z) = a_R(z) + ia_I(z) = |a(z)|e^{i\phi(z)}$ evaluated at many discrete sites z. The dimensionless coordinate z is the ratio $Z/N\lambda$ where the "slippage distance" $N\lambda$ is defined by the number of optical wavelengths that pass over a resonant electron as that electron traverses the undulator length L. With the slowly-varying amplitude and phase approximation, and the coordinate change $Z \rightarrow Z + ct$, the wave operator reduces to a single derivative in time. The dimensionless optical field envelope is $a(z) = 4\pi NeKLE(z)/\gamma_0^2 mc^2$ where $E(z)$ is the complex optical electric field, and $\gamma_0 mc^2$ is the resonant electron energy, $\gamma_0^2 = k(1+K^2)/2k_0$. Simulations take place within a window of width W along z that is an integral number of slippage distances long. At any τ, electrons at coordinate $z + \tau$ in the electron beam overlap the light at coordinate z in the optical wave. The electron phase relative to the optical wave and undulator fields is $\zeta = (k+k_0)Z - \omega t$, and the phase velocity is $v = \dot{\zeta} = L[(k+k_0)\beta_z - k]$. The self-consistent electron and optical equations [24] are

$$\dot{v}(z+\tau) = [\,1 - v(z+\tau)/2\pi N\,]^2 \left(a_R(z)\cos(\zeta(z+\tau)) - a_I(z)\sin(\zeta(z+\tau)) \right) \tag{1}$$

$$\dot{\zeta}(z+\tau) = v(z+\tau) \tag{2}$$

$$\dot{a}_R(z) = -j(z+\tau) < [\,1 - v(z+\tau)/2\pi N\,]^{1/2} \cos(\zeta(z+\tau)) > \tag{3}$$

$$\dot{a}_I(z) = j(z+\tau) < [\,1 - v(z+\tau)/2\pi N\,]^{1/2} \sin(\zeta(z+\tau)) > \tag{4}$$

where the dimensionless current density is $j(z) = 8N(e\pi KL)^2 \rho(z)/\gamma_0^3 mc^2$, $\rho(z)$ is the actual particle density at site z, time derivatives are with respect to the dimensionless time τ, and $<...>$ is an average over sample electrons at site $z + \tau$ in the electron beam.

In order to maintain strong coupling between the electrons and light, the phase velocity ν cannot be too far from resonance, $\nu = 0$. The initial resonance condition $\nu(\tau=0) = \nu_0$ is taken to be at the maximum of the weak-field gain spectrum. In both the amplifier and oscillator cases, we start the optical field at low values $a(\tau=0) = a_0$, well below saturation. The dimensionless current density j represents low single-pass gain when $j \approx 1$, and high gain when $j \gg 1$. Typically, the FEL oscillator configuration uses $j \approx 1$, while the FEL amplifier configuration uses $j \gg 1$. Weak optical fields give values of $|a| < \pi$, while strong fields give values of $|a| > \pi$. For small current and weak fields, maximum gain is at $\nu_0 = 2.6$; for large current and weak fields, maximum gain is at $\nu_0 = 0$. The electron beam at each z has a uniform distribution of initial phases $\zeta(\tau=0)$ over a 2π range so that the initial optical phase is arbitrary; we take $\phi(\tau=0) = 0$ at each z. The factors $[1-\nu/2\pi N]$ in (1)-(4) are close to unity unless the electrons lose a significant fraction of their energy and become less relativistic. Electron motion in terms of ν corresponds to changes in the electron energy through the relation $\nu \simeq 4\pi N(\gamma - \gamma_0)/\gamma_0$. We take $N = 50$ in our examples as a common value typical of both amplifiers and oscillators. The final optical power spectrum $P(k)$ is made more relevant by expressing k, the optical wavenumber, in terms of the corresponding resonance parameter $\nu(k)$; similarly, the electron distribution function $f(\gamma)$ is expressed in terms of $\nu(\gamma)$. The power spectrum $P(\nu(k))$ and the electron distribution function $f(\nu(\gamma))$ are more physically meaningful in terms of their affect on the resonance condition.

The single-mode version of (1)-(4) is obtained by removing all z dependence; all sites are given the same initial values of ζ_0, ν_0, and $a(z) = a_0$. An estimate of the trapped-particle motion is obtained by considering the electrons in harmonic orbits near the stable fixed-point $\zeta^* = \pi/2$. With j not too large, and and small energy extraction ($N >> 1$), $|a|$ remains approximately constant during the synchrotron oscillations at saturation. Then, the motion of a trapped electron is $\zeta(\tau) = \zeta^* + (\nu_0/\nu_S)\sin(\nu_S\tau)$ with the initial position (ζ^*, ν_0). The synchrotron or trapped-particle oscillation frequency is $\nu_S = a_0^{1/2}$. When the trapped electrons oscillate through a synchrotron cycle, part of the current driving the optical field in (3) and (4) also oscillates through one cycle. It is the oscillation of the driving phase in the average <...> that causes the trapped-particle frequency to be imposed on the optical wave as it slips over electrons. The sidebands appear at $\nu_0 \pm \nu_S$, so that the new FEL power is shifted from the fundamental wavelength by $\Delta\lambda/\lambda = \nu_S/2\pi N$. The shift has a simple interpretation; $\Delta\lambda/\lambda$ = "the number of synchrotron oscillations"/ "the number of undulator periods".

3. The Trapped-Particle Instability in Short-Pulse Oscillators

An FEL oscillator that is powered by an RF accelerator injects a series of short picosecond electron pulses into the undulator while the optical pulse bounces between mirrors separated by a distance $S > L$. High-power saturation is reached after many passes, and the FEL continues to work for an additional 10^3 to 10^4 passes. The current density of each short pulse $j(z)$ is taken to be parabolic with the form $j(z) = j\ (1 - 2z^2/\sigma_z^2)$ for $|z| < \sigma_z/\sqrt{2}$ and $j(z)=0$ for $|z| > \sigma_z/\sqrt{2}$; the length σ_z is normalized by the slippage distance $N\lambda$. Typically, RF accelerators produce current densities which give values of j in the moderate range $1 \rightarrow 100$ and $\sigma_z = 1 \rightarrow 30$. The loss on each pass (due to mirror absorption and transmission) is described by $e^{-n/Q}$ where n is the pass number. Usually, Q is from $2 \rightarrow 200$.

The repetition frequency of successive electron pulses must be matched to the bounce frequency of the light pulse, $2Sc$. When synchronized, each new electron pulse arrives at the beginning of the undulator simultaneous to the rebounding optical pulse. The "desynchronism," $d = 2\Delta S/N\lambda$, is the displacement between the pulses after each pass when the mirrors are separated by $S - \Delta S$. If $|d|$ is too large, the electron and optical pulses do not overlap for a sufficient number of passes and the FEL operates below threshold coupling. If $d = 0$, exact synchronism, the FEL is also below threshold [5-7,11-14,21] due to an effect termed "laser lethargy" [12]. Because of slippage, gain is preferentially deposited on the trailing edge of the optical pulse causing the optical pulse centroid to travel slower than c in vacuum; therefore, the optical bounce frequency $2Sc$ is overestimated. To compensate for the "lethargic" light, the path S must be reduced by operating at $d > 0$.

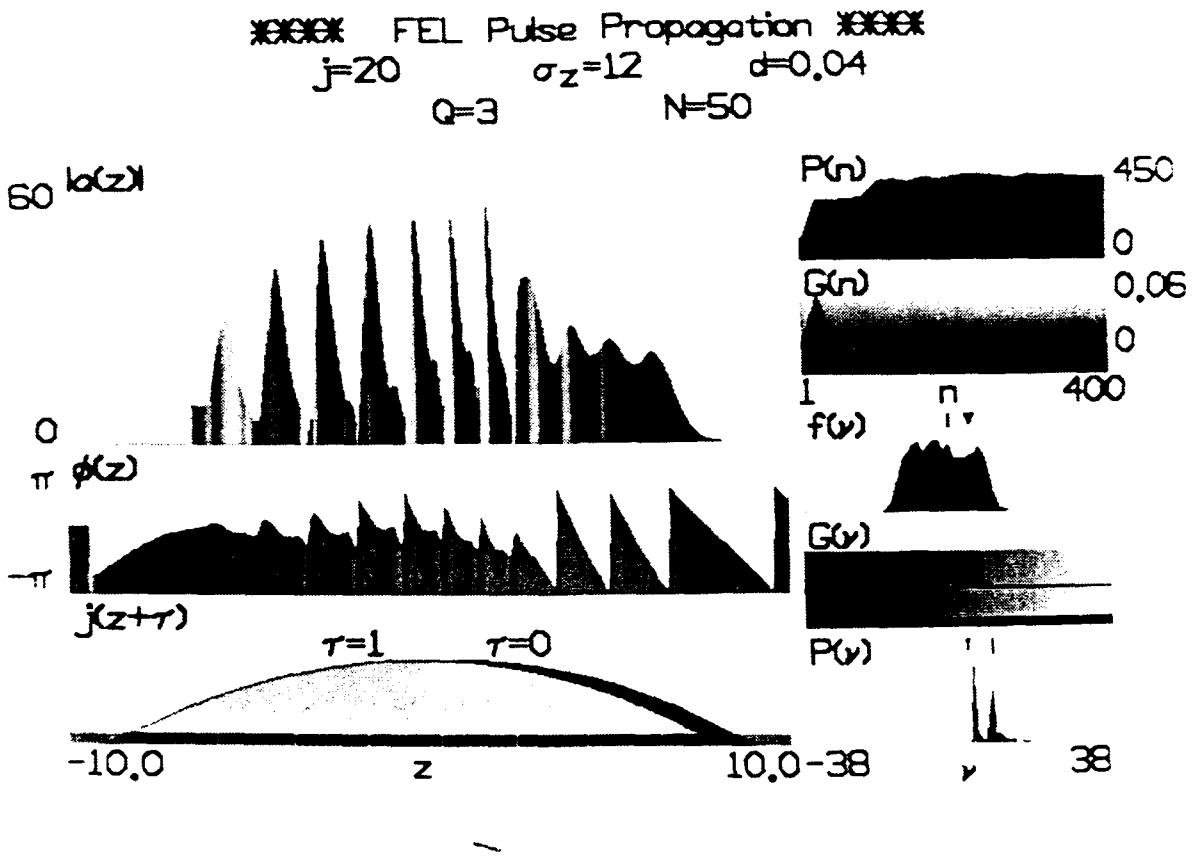

Fig. 1. Driven by the short electron pulse $j(z+\tau)$, the trapped-particle instability has modulated the optical pulse envelope $a(z)$ at the synchrotron period $\nu_S \approx 2\pi$. The total optical power $P(n)$ and gain $G(n)$ reach steady-state after n=400 passes through the oscillator. $G(\nu)$ is the weak-field gain spectrum, included for reference. The final optical power spectrum $P(\nu)$ has an additional sideband at $\nu_0 + \nu_S$ due to the instability. The final electron distribution $f(\nu)$ is broad because of the strong fields.

A short-pulse simulation is shown in Fig. 1. Steady-state is reached after $n = 400$ passes with moderately high current $j = 20$, an intermediate pulse length $\sigma_z = 12$, $N = 50$, desynchronism $d = 0.04$, and $Q = 3$. Large output coupling is used (low Q) because the gain is far above threshold. The top right figure follows the power $P(n)$ averaged over the whole window. Second on the right is the net gain $G(n)$ experienced by the pulse each pass. The lower left picture shows the electron pulse shape before ($\tau = 0$) and after ($\tau = 1$) the slippage of one unit per pass in a window of width $W = 20$. The upper left figures show the final optical field amplitude $|a(z)|$ and the optical phase profile $\phi(z)$ plotted along z where $-W/2 < z < W/2$. The jumps in phase of 2π are meaningless, but the slope of the phase profile indicates a local change in the laser light

wavenumber and a resonance change $\Delta\nu(k) = -\phi'(z)$ away from ν_0. The grey scale on $\phi(z)$ shows the local frequency component matching the gain spectrum $G(\nu)$ on the right. The grey scale superimposed on the field amplitude shows the local gain experienced by each part of $a(z)$ on the last pass in the undulator. This grey scale matches the scale in $G(n)$ pictured on the right. Third on the right is the final electron distribution $f(\nu)$, and fifth is the final optical power spectrum $P(\nu)$ found from the Fourier transform of $a(z)$. The fourth picture $G(\nu)$ is the weak-field gain spectrum for the current density $j = 20$.

The simulation has reached saturation with peak fields near $|a| \approx 60$. Each pass, those electrons near the center of the pulse, that become trapped, encounter fields strong enough to cause about one synchrotron oscillation since $\sqrt{a} \approx 2\pi$. Normal saturation takes place early and the power is steady for about 50 passes; then the power increases again as the sideband grows. Strong optical fields and the resulting trapped-particle oscillations must occur before there is significant gain at the sideband frequency ν_S. The extra power is in the sidebands and the fundamental remains saturated [17,23]. A simple calculation shows that the field component at the sideband frequency grows as $a(\tau) = a_S \exp((j/4\nu_S)^{1/2}\tau)$ where $\nu_S = |a|^{1/2}$ at saturation, and a_S is the initial sideband field at ν_S. In this simulation, $(j/4\nu_S)^{1/2} \approx 0.8$ and the loss rate is $-(2Q)^{-1} \approx -0.2$, so the sideband gain is above threshold. The sideband structure is clear in $|a(z)|$, and the power spectrum $P(\nu)$. The modulation length is close to the slippage distance indicating $\nu_S \approx 2\pi$, and the sideband in $P(\nu)$ occurs at $\Delta\nu \approx 2\pi$ above the fundamental. The full-width of the electron distribution is given by the height of the closed-orbit region in phase-space, $4|a|^{1/2}$.

The characteristics of the trapped-particle instability in short-pulse FELs are briefly outlined below [21]. Most characteristics have now been confirmed by experiments [1,8,11].

1. At small $d>0$, the FEL usually reaches power levels large enough to cause the trapped-particle instability. This gives a broad, possibly chaotic, optical power spectrum, and a broad electron distribution.

2. At large d, the steady-state power is small due to the reduced coupling, and the trapped-particle instability is less likely to occur. The final optical power spectrum is narrow and in a single-mode; the final electron distribution is narrow due to the weak optical fields.

3. When d is in the intermediate range, we have often observed limit-cycle behavior in the simulations [5,6,13,21]. In this case, the pulse continually changes shape while the trapped-particle instability creates new subpulses.

4. Increasing the current density j or the resonator Q increases the steady-state power, the synchrotron frequency, and the sideband gain. The addition of sideband power is cumulative, since the presence of a strong sideband again increases the steady-state power.

5. If taper is introduce into the undulator design, the synchrotron frequency is only slightly modified, and the sideband gain is reduced [13,22,23].

6. When the pulse length σ_z is near unity, the short-pulse effects can be dramatic [11]. Since the sideband modulation first appears near the slippage distance, a short pulse may not be long enough to support modulation at the synchrotron frequency. The optical pulse can be made significantly shorter or longer than the picosecond electron pulse by adjusting d.

4. Simulations in a "Wrapped-Window"

If the electron pulse is not short ($\sigma_z >> 1$) it is prudent to simulate the FEL by sampling a smaller window $W << \sigma_z$ with periodic boundary conditions such that $\zeta(z - W/2) = \zeta(z + W/2)$; these can be called "wrapped-window" simulations [17,22,23]. Using a number of sites N_W in a window of width W we follow a restricted number of modes $\nu_l = \nu_0 - (2\pi/W)(l - N_W/2)$ where $l = 0, 1, 2, ..., N_W - 1$; the mode spacing is $\Delta\nu = 2\pi/W$. The desynchronism d and the pulse length σ_z don't enter the problem, and the current density $j(z) = j$ is constant along the window.

The FEL simulation in Fig. 2 uses $j = 20$, $Q = 3$, and $N = 50$ (as in Fig. 1), but for a long pulse $\sigma_z >> W = 4$. The individual pictures are the same as in Fig. 1 except for the reference to pulse shape. Without some noise source, no power would develop at frequencies other than the fundamental and every site z would evolve identically. Specific sources of noise can vary from one experiment to the next. In Fig. 2, the initial electron phases are uniformly spread over a 2π range, but with an additional random phase of zero mean and standard deviation $\delta\zeta \approx 1.0 \times 10^{-6}$. Electron shot noise is a typical source of this kind of noise. In the pulse simulations no random noise is introduced, since the spectral features of $j(z)$ are sufficient. After $n = 400$ passes, the steady-state optical fields peak at $|a| \approx 60$ just as in Fig. 1, and the final power spectrum $P(\nu)$ is similar to Fig. 1, but without the short pulse features.

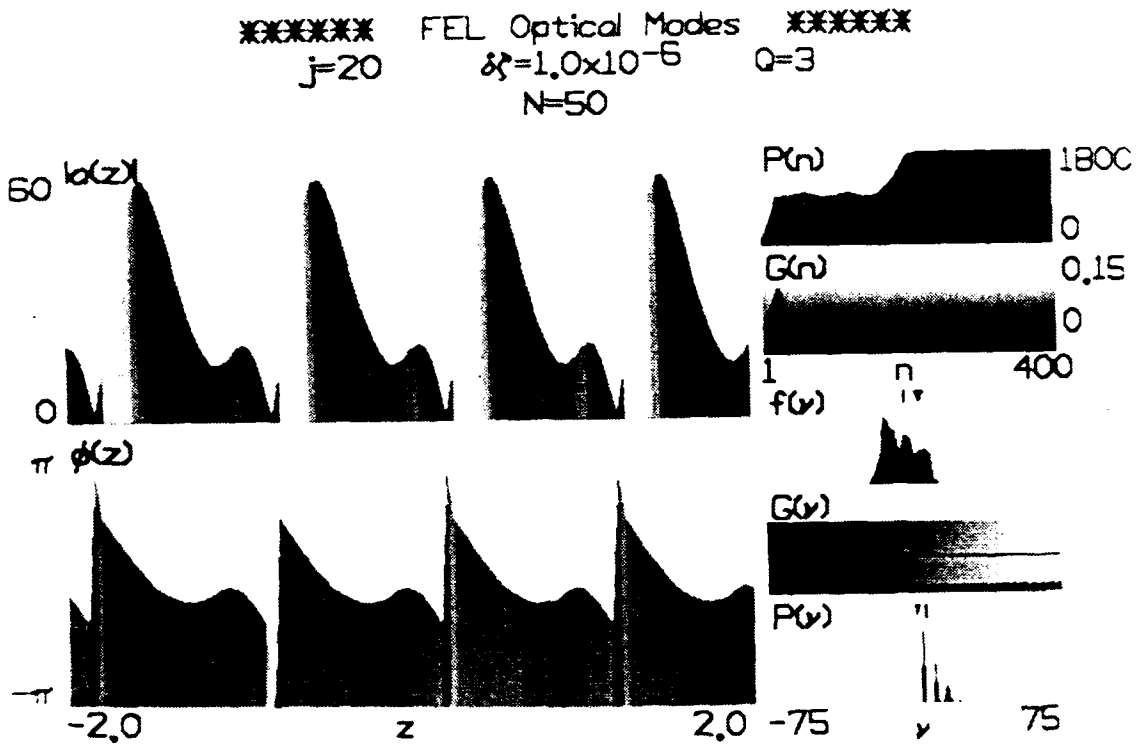

Fig. 2. The "wrapped-window" simulation gives a clear example of the trapped-particle instability in the FEL oscillator without the complicating features of short pulses.

Wrapped-window simulations have many of the same characteristics as for pulses, but without the effects of desynchronism. As $\sigma_z \to \infty$ the wrapped-window approach is the only viable solution to the FEL multimode simulation.

1. Increases in j or Q make the trapped-particle instability more severe. It is unusual to find the periodic, even modulation shown in Fig. 2.
2. When there is taper in the undulator design, the instability is less prominent for the same reasons as stated in the pulse case.

3. Over many hundreds of passes, the stored optical wave "sees" many synchrotron oscillations, so that any sideband gain above threshold gives large growth from a small amount of noise. The resulting steady-state features are therefore not affected by the details of the noise source employed.

5. The Trapped-Particle Instability in High-Current FEL Amplifiers

In the high-current FEL amplifier, $j>>1$, large optical power can be produced in a single pass through the undulator. An induction linac accelerator and a long undulator can result in values $j = 10^4 \rightarrow 10^5$ [2]. The electron pulses are long, $\sigma_z \rightarrow \infty$, so that the wrapped-window simulation method is essential. The FEL growth rates are so large that electrons become trapped early in the undulator and begin executing synchrotron oscillations. There can be from several to many tens of synchrotron oscillations along the undulator so that the optical field experiences far fewer synchrotron cycles than in the oscillator case. However, even the limited number of synchrotron cycles can result in significant sideband gain owing to the large current density j.

The wrapped-window simulation in Fig. 3 follows the power and gain from $\tau = 0 \rightarrow 1$ for an FEL with high current $j = 8\times10^4$, an initial field $a_0 = 20$ starting at $\nu_0 = 0$, and $N = 50$. No electron phase noise is present, but a small initial sideband field $a_S = 0.01$ is introduced at $\nu_S = 20\pi$. Spontaneous emission or electron shot noise from the trapped electrons can lead to a contribution of this size because j is large. The power $P(\tau)$ and gain $G(\tau)$ are seen to oscillate with the synchrotron frequency $\nu_S \approx 20\pi$ and impose a strong modulation on the light wave envelope $a(z)$. The final power spectrum $P(\nu)$ shows that the sideband has grown to almost equal the fundamental power.

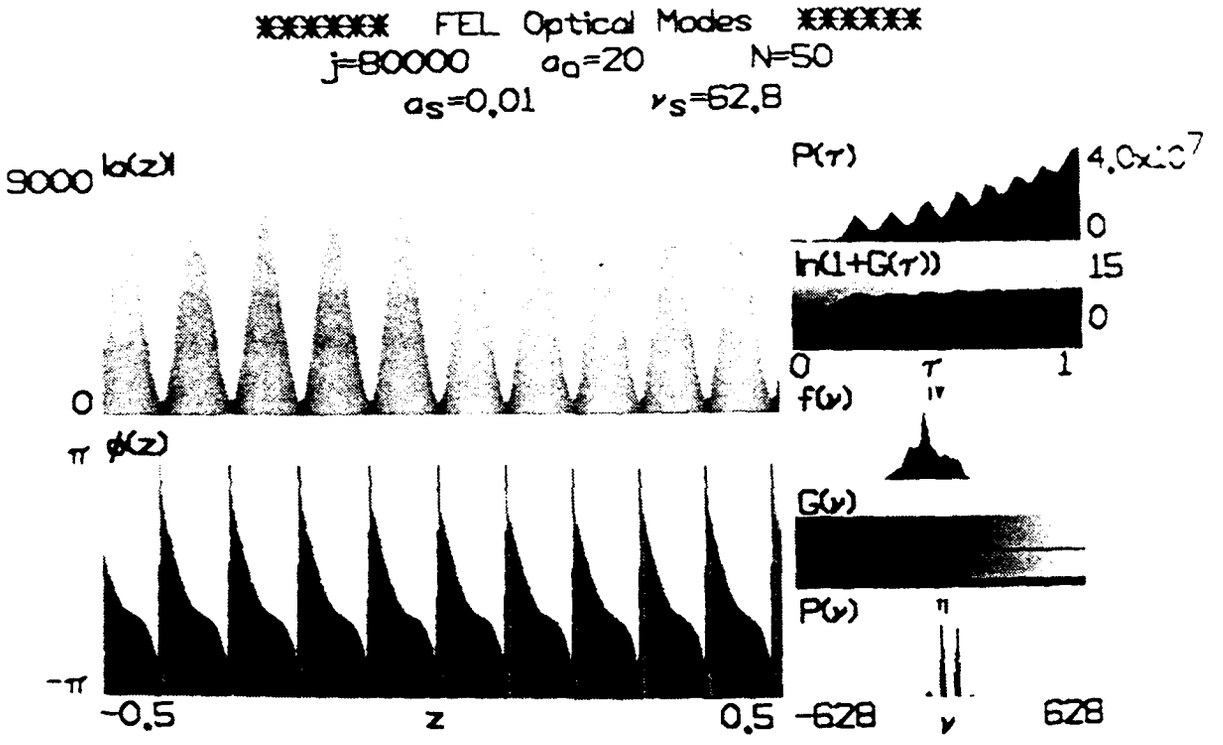

Fig. 3. The trapped-particle instability can create significant sideband power during one pass in the FEL amplifier. The high-currents used in amplifiers give much stronger optical fields at early stages of the undulator that can cause several synchrotron oscillations, and impose a corresponding modulation onto the optical wave envelope. In this example, the sideband is spaced at $\nu_S \approx 20\pi$.

The trapped-particle instability in FEL amplifiers differs in many ways from the oscillator case. Sources of noise are much more important, and there is no resonator Q to consider.

1. Large current j makes the trapped-particle instability more likely. Using the sideband growth rate, we can evaluate the current j^* needed to make the sideband field a_S equal to the fundamental, $a_0 = \nu_S^2$. This gives

$$j^* = 16\nu_S \ln^2(\nu_S/\sqrt{a_S}) \quad .$$

The current j^* has a slow logarithmic dependence on the initial sideband field a_S so that an accurate estimate is not too crucial; we take $a_S = 0.01$. We also estimate that there must be at least a few synchrotron oscillations, say $\nu_S \approx 16\pi$, before the optical wave could accurately determine the synchrotron frequency. This gives a characteristic current density $j^* \approx 3\times10^4$ where sidebands could be expected to significantly alter the final FEL amplifier spectrum.

2. In the tapered undulator case, less current is trapped, and the synchrotron oscillations have a smaller amplitude so that the trapped-particle instability is observed to be less severe, as in FEL oscillators.

3. Input noise at the sideband frequency is important to the development of significant sideband power in FEL amplifiers. Shot noise and spontaneous emission cannot be eliminated, and may be a significant contribution at large current densities.

4. For the large currents $j > j^*$, the FEL does not reach steady-state operation even in strong optical fields $|a|$. The power continues to increase and so does the synchrotron frequency. This continual change in the synchrotron frequency may play a useful role in suppressing the growth at any particular sideband frequency.

In conclusion, we find that the trapped-particle instability is more difficult to suppress in the FEL oscillator than in the FEL amplifier. The large number of synchrotron oscillations experienced by the light stored in the oscillator make the effective gain over for many passes large. But, while the trapped-particle instability has already been observed in the FEL oscillator, it has not yet been found in the FEL amplifier. The many differences between FEL oscillator and amplifier simulations implies that we should not use the oscillator case as a direct proof that there will be an equally prominent instability in real FEL amplifiers.

Acknowledgments

The author is grateful for support from Naval Research Lab Contract No. N00014-86-C-2006, the U.S. Office of Naval Research Contract No. N00014-85-C-0493, and the U.S. Air Force Office of Scientific Research Contract No. F49620-85-C-0087.

References

[1] B. E. Newman, R. W. Warren, R. L. Sheffield, W. E. Stein, M. T. Lynch, J. S. Fraser, J. C. Goldstein, J. E. Sollid, T. A. Swann, J. M. Watson, and C. A. Brau, IEEE Journal of Quantum Electronics, **QE-21**, 867 (1985).

[2] T. J. Orzechowski, E. T. Scharlemann, B. Anderson, V. K. Neil, W. M. Fawley, D. Prosnitz, S. M. Yarema, D. B. Hopkins, A. C. Paul, A. M. Sessler and J. S. Wurtele, IEEE Journal of Quantum Electronics, **QE-21**, 831 (1985).

[3] N. M. Kroll and M. N. Rosenbluth, *"Physics of Quantum Electronics,"* 7, 147 (1980).

[4] N. M. Kroll, P. L. Morton, and M. N. Rosenbluth, *"Physics of Quantum Electronics,"* 7, 89 (1980).

[5] W. B. Colson and S. K. Ride, *"Physics of Quantum Electronics,"* 7, 377 (1980).

[6] W. B. Colson, International Summer School of Quantum Electronics, Erice (Sicily), eds. S. Martellucci and A. N. Chester, Plenum Press (1980), p. 189.

[7] G. Dattoli, A. Marino, A. Renieri and F. Romanelli, IEEE Journal of Quantum Electronics, **QE-17**, 1371 (1981).

[8] J. A. Edighoffer, G. R. Neil, C. E. Hess, T. I. Smith, S. W. Fornaca, H. A. Schwettman, Phys. Rev. Lett. **52**, 344 (1984).

[9] N. M. Kroll, P. L. Morton and M. N. Rosenbluth, IEEE Journal of Quantum Electronics, **QE-17**, 1436 (1981).

[10] J. C. Goldstein and W. B. Colson, Proc. of the Int. Conf. on Lasers '81, ed. C.B. Collins (STS Press, McLean, VA, 1981), p. 93.

[11] J. N. Eckstein, J. M. J. Madey, K. Robinson, T. I. Smith, S. Benson, D. Deacon, R. Taber, and A. Gaupp, *"Physics of Quantum Electronics,"* **8**, 49 (1982).

[12] H. Al-Abawi, J. K. McIver, G. T. Moore, and M. O. Scully, *"Physics of Quantum Electronics,"* **8**, 415 (1982).

[13] W. B. Colson, *"Physics of Quantum Electronics"*, **8**, 457 (1982).

[14] G. Dattoli, A. Marino, and A. Renieri, *"Physics of Quantum Electronics,"* **8**, 515 (1982).

[15] A. T. Lin, *"Physics of Quantum Electronics,"* **9**, 867 (1982).

[16] J. C. Goldstein and W. B. Colson, Proc. Int. Conf. LASERS '82, New Orleans, LA, Dec. 13-17, p. 218 (1982), ed. R. C. Powell.

[17] W. B. Colson and R. A. Freedman, Opt. Commun., **40**, 37 (1983).

[18] J. C. Goldstein, *"Free Electron Generators of Coherent Radiation,"* eds. C. A. Brau, S. F. Jacobs and M. O. Scully, SPIE **453**, 2 (1983).

[19] H. Freund, P. Sprangle, and C.-M. Tang, Phys. Rev. A**25**, 3121 (1982).

[20] M. N. Rosenbluth, H. V. Wong, and B. N. Moore, *"Free Electron Generators of Coherent Radiation,"* eds. C. A. Brau, S. F. Jacobs and M. O. Scully, SPIE **453**, 25 (1983);
N. M. Kroll, M. N. Rosenbluth, H. V. Wong, B. N. Moore, and S. Tsunoda, Conf. on Lasers and Electro-Optics, CLEO/IQEC '84, Anahiem CA (May 1984);

[21] W. B. Colson and A. Renieri, J. de Physique **44**, C1-11 (1983).

[22] W. B. Colson, *"Free Electron Generators of Coherent Radiation,"* eds. C. A. Brau, S. F. Jacobs and M. O. Scully, SPIE **453**, 289 (1983).

[23] R. A. Freedman and W. B. Colson, Opt. Commun., **52**, 409 (1985).

[24] W. B. Colson and S. K. Ride, Phys. Lett. A**76**, 379 (1980).